



Solid state water motions revealed by deuterium relaxation in $^2\text{H}_2\text{O}$ -synthesized kanemite and $^2\text{H}_2\text{O}$ -hydrated Na^+ -Zeolite A

Bernie O'Hare^a, Michael W. Grutzeck^b, Seong H. Kim^c, David B. Asay^c, Alan J. Benesi^{a,*}

^a Department of Chemistry, The Pennsylvania State University, The NMR Facility, Room 008, The Chemistry Building, University Park, PA 16802, USA

^b Materials Research Laboratory, The Pennsylvania State University, University Park, PA 16802, USA

^c Department of Chemical Engineering, The Pennsylvania State University, University Park, PA 16802, USA

ARTICLE INFO

Article history:

Received 2 May 2008

Revised 7 August 2008

Available online 3 September 2008

Keywords:

Deuterium NMR

NMR relaxation

Water

Hydrates

NMR

Quadrupolar relaxation

Kanemite

Zeolite A

Chemical exchange

ABSTRACT

Deuterium NMR relaxation experiments, low temperature deuterium NMR lineshape analysis, and FTIR spectra are consistent with a new model for solid state jump dynamics of water in $^2\text{H}_2\text{O}$ -synthesized kanemite and $^2\text{H}_2\text{O}$ -hydrated Na^+ -Zeolite A. Exchange occurs between two populations of water: one in which water molecules are directly coordinated to sodium ions and experience C_2 symmetry jumps of their OH bonds, and a population of interstitial water molecules outside the sodium ion coordination sphere that experience tetrahedral jumps of their OH bonds. For both samples the C_2 jump rate is much faster than the tetrahedral jump rate. ^2H NMR relaxation experiments match well with the fast exchange regime of the model over a wide range of temperatures, including room temperature and above. For hydrated Zeolite A, the kinetic activation parameters for the tetrahedral and C_2 symmetry jumps are $\Delta H_{\text{tet}}^\ddagger = +17$ kJ/mol, $\Delta S_{\text{tet}}^\ddagger = -109$ J/(mol K), $\Delta H_{C_2}^\ddagger = +19$ kJ/mol, and $\Delta S_{C_2}^\ddagger = -20$ J/(mol K). For kanemite, $\Delta H_{\text{tet}}^\ddagger = +23$ kJ/mol, $\Delta S_{\text{tet}}^\ddagger = -69$ J/(mol K), $\Delta H_{C_2}^\ddagger = +23$ kJ/mol, and $\Delta S_{C_2}^\ddagger = -11$ J/(mol K).

© 2008 Elsevier Inc. All rights reserved.

1. Introduction

Evidence from deuterium NMR and infrared spectroscopy shows that solid state water exists at ambient temperatures in a variety of $^2\text{H}_2\text{O}$ -hydrated porous silicates [1–3]. The NMR evidence is based on the sharp $^2\text{H}_2\text{O}$ resonance observed in the deuterium spectrum and its extremely short and field dependent deuterium NMR T_1 values. Both characteristics were previously shown to be consistent with tetrahedral jumps of the $\text{O}-^2\text{H}$ bonds on a fixed lattice rather than liquid state isotropic rotational diffusion. In this paper a more detailed model is proposed for $^2\text{H}_2\text{O}$ -synthesized kanemite ($\text{Na}^+\text{HSi}_2\text{O}_5 \cdot 3^2\text{H}_2\text{O}$) and $^2\text{H}_2\text{O}$ -hydrated Na^+ -Zeolite A. The experimental data support this model over a wide range of temperatures from below room temperature to above the boiling point of pure water at atmospheric pressure.

^2H NMR is particularly advantageous for characterization of angular dynamics because it is dominated by the single nucleus ^2H quadrupolar interaction. The strong quadrupolar interaction, arising from the coupling of the electric field gradient tensor with the nuclear electric quadrupole moment Q , dominates the much weaker ^2H chemical shift and dipolar interactions [4,5]. For ^2H in various “rigid” solids, the deuterium qcc ($q_{\text{cc}} \equiv e^2qQ/h$) varies from

160 to 340 kHz with $0 \leq \eta \leq 0.15$. The small η values indicate nearly axial symmetry of the electric field gradient tensor, with the V_{zz} axis parallel to the $\text{X}-^2\text{H}$ covalent bond. This holds true for water, where the electric field gradient tensor in $^2\text{H}_2\text{O}$ has nearly axial symmetry about the $\text{O}-^2\text{H}$ covalent bond axis. Therefore, the spectrum and relaxation times for $^2\text{H}_2\text{O}$ can be used to monitor the time dependence of the angle made by the $\text{O}-^2\text{H}$ covalent bond with the magnetic field [1,6]. A repertoire of deuterium NMR techniques are sensitive to $\text{O}-^2\text{H}$ motions with frequencies (ν_{motion}) of $1 \times 10^{-2} < \nu_{\text{motion}} < 1 \times 10^{15} \text{ s}^{-1}$ [7,8]. These encompass most of the range of frequencies of reorientational and translational motions of water and other molecules in condensed phases.

For bulk liquid and supercooled liquid water, the ^2H T_1 and T_2 relaxation times show that the $\text{O}-^2\text{H}$ bonds experience isotropic rotational diffusion. At 292 K and atmospheric pressure, the rotational rate constant for liquid $^2\text{H}_2\text{O}$ is $2.8 \times 10^{11} \text{ s}^{-1}$ ($=6 D_{\text{rot}}$, where D_{rot} is the rotational diffusion coefficient) [1], while for supercooled liquid water at high pressures and cold temperatures the rotational rate constants are several orders of magnitude lower [8,9]. Although it occurs in some solids with spherically symmetric molecules [10], isotropic rotational diffusion is typical of liquids. In contrast, for pure solid *Ice I_h* at atmospheric pressure, ^2H NMR lineshape analysis and stimulated echo experiments show that the $\text{O}-^2\text{H}$ bonds experience tetrahedral jumps (jumprate $\sim 10^4 \text{ s}^{-1}$ several °C below freezing) due to the diffusion of Bjerrum defects

* Corresponding author. Fax: +1 814 865 3314.

E-mail address: alan@chem.psu.edu (A.J. Benesi).

through the ice lattice [6,11]. On a slower time scale, there is also a seven site reorientation mediated by proton transfer and interstitial translational diffusion. For most *crystalline hydrates*, variable temperature ^2H NMR lineshape analysis shows that the $\text{O}-^2\text{H}$ bonds experience rapid C_2 symmetry jumps around the bisector of the HOH bond angle with jump rates $\geq 10^6 \text{ s}^{-1}$ at ambient temperatures [12,13]. In a few cases, spectral analysis for *crystalline hydrates* shows that the water molecules are *rigid* on the “NMR timescale” ($\nu_{\text{jumps}} \ll \text{qcc}$) except for librations that reduce the effective ^2H qcc. ^2H NMR stimulated echo experiments on tetrahydrofuran *clathrate hydrate* show that the $\text{O}-^2\text{H}$ bonds of the water molecules experience *tetrahedral jumps* (ascribed to Bjerrum defects) on a distorted tetrahedral lattice as well as a slower randomization process ascribed to a combination of Bjerrum and ionic defects [14]. Dynamics characterized by rigidity or jumps provides atomic level evidence of the solid state.

Recent ^2H NMR studies in our laboratories have found solid state water at room temperature and higher in the layered silicate kanemite synthesized with $^2\text{H}_2\text{O}$ and in the nearly spherical porous cavities of $^2\text{H}_2\text{O}$ -hydrated Na^+ -Zeolite A [1]. Unlike crystalline hydrates and clathrates, however, in these samples the solid state water extends several layers away from the silicate or aluminosilicate solid surface. Here we propose a more complete model for the dynamics in these hydrated solids that is consistent with variable temperature quadrupole echo spectra obtained at lower temperatures and with the experimental deuterium T_1 and T_2 relaxation times over a range of temperatures from below 273 K to as high as 418 K. In the model, water molecules directly coordinated to Na^+ experience C_2 symmetry jumps of their $\text{O}-^2\text{H}$ covalent bonds and water molecules outside the direct coordination sphere of Na^+ experience tetrahedral jumps of their $\text{O}-^2\text{H}$ covalent bonds.

2. Theory

2.1. Calculation of the T_1 and T_2 relaxation times

The theoretical calculations use the conventions of Mehring [5] and are based on the formalism developed by Torchia and Szabo [15]. The observed deuterium T_1 and T_2 values are given by [16,17]:

$$\frac{1}{T_1} = \frac{\omega_Q^2}{3} (J_1(\omega) + 4J_2(2\omega)) \quad (1a)$$

$$\frac{1}{T_2} = \frac{\omega_Q^2}{3} \left(\frac{3}{2}J_0(0) + \frac{5}{2}J_1(\omega) + J_2(2\omega) \right) \quad (1b)$$

where $\omega_Q = \frac{3e^2qQ}{4h}$, ω is the Larmor frequency in radians/s, and $J_0(0)$, $J_1(\omega)$ and $J_2(2\omega)$ are the spectral densities at integer multiples of the Larmor frequency that depend on the details of the molecular motion. We have omitted the superscripts in the $J_n(\omega)$ indicating $l=2$ to simplify the notation. The derivation of the spectral densities for the several models considered here is available upon request.

2.2. Spectral densities for isotropic rotational diffusion

The dynamic model that applies to liquid state water is small step isotropic rotational diffusion (IRD). The spectral densities are well known, and are given by [18,19]:

$$J_0^{\text{IRD}}(0) = \frac{1}{5} \left(1 + \frac{\eta^2}{3} \right) \frac{2}{6D_{\text{rot}}} \quad (2a)$$

$$J_1^{\text{IRD}}(\omega) = \frac{1}{5} \left(1 + \frac{\eta^2}{3} \right) \frac{12D_{\text{rot}}}{(6D_{\text{rot}})^2 + \omega^2} \quad (2b)$$

and

$$J_2^{\text{IRD}}(2\omega) = \frac{1}{5} \left(1 + \frac{\eta^2}{3} \right) \frac{12D_{\text{rot}}}{(6D_{\text{rot}})^2 + 4\omega^2} \quad (2c)$$

where $J_m^{\text{IRD}}(m\omega) = J_{-m}^{\text{IRD}}(-m\omega)$. With $6D_{\text{rot}} = 1/\tau_c$ and Eq. (3), these expressions yield the same results derived by Sudmeier et al. [20].

2.3. Spectral densities for tetrahedral jumps

Using the appropriate correlation functions and jump matrix, we find the tetrahedral jump spectral densities in the *laboratory* reference frame [21]:

$$\begin{aligned} J_0^{\text{tet}}(0) = & (9(3744 + \eta(-864 + 871\eta)) + (2016 + \eta(480 + 341\eta)) \\ & \times \cos[4\beta] + 648\eta^2 \cos[4\alpha] \sin[\beta]^4 + 4 \cos[2\beta] \\ & \times (288 + \eta(-5856 + 851\eta) - 432\eta(3 + \eta)) \\ & \times \cos[2\alpha] \times \sin[\beta]^2) + 64(3 + \eta) \sin[\beta]^2 (-81\eta \cos[2\alpha] \\ & + 2\sqrt{2}(-12 + 5\eta) \cos[3\alpha] \sin[2\beta])) \div (331776k_{\text{tet}}) \quad (3a) \end{aligned}$$

$$\begin{aligned} J_1^{\text{tet}}(\omega) = & \frac{1}{5184(\omega^2 + 16k_{\text{tet}}^2)} ((-4(288 + \eta(-672 + 149\eta)) \\ & \times \cos[2\beta] - (2016 + \eta(480 + 341\eta)) \cos[4\beta] - 256 \\ & \times \sqrt{2}(3 + \eta)(-12 + 5\eta) \cos[3\alpha] \cos[\beta] \sin[\beta]^3 \\ & + 9(864 + \eta(96 + 161\eta) + 24\eta(-3\eta \cos[4\alpha] \sin[\beta]^4 \\ & + 4(3 + \eta) \cos[2\alpha] \sin[2\beta]^2)))k_{\text{tet}} \quad (3b) \end{aligned}$$

$$\begin{aligned} J_2^{\text{tet}}(2\omega) = & \frac{1}{82944(4k_{\text{tet}}^2 + \omega^2)} (k_{\text{tet}}(9(3744 + \eta(-864 + 871\eta)) \\ & + (2016 + \eta(480 + 341\eta)) \cos[4\beta] + 648\eta^2 \cos[4\alpha] \\ & \times \sin[\beta]^4 + 4 \cos[2\beta](288 + \eta(-5856 + 851\eta) - 432\eta \\ & \times (3 + \eta) \cos[2\alpha] \sin[\beta]^2) + 64(3 + \eta) \sin[\beta]^2 (-81\eta \cos[2\alpha] \\ & + 2\sqrt{2}(-12 + 5\eta) \cos[3\alpha] \sin[2\beta])) \quad (3c) \end{aligned}$$

where k_{tet} is the tetrahedral jump rate constant in s^{-1} , η is the asymmetry parameter, and $\alpha = \alpha_{\text{CL}}$ and $\beta = \beta_{\text{CL}}$ are the (powder average) Euler angles (we choose $\gamma_{\text{CL}} = 0$ with no loss of generality) relating the crystal reference frame to the laboratory reference frame, i.e. magnetic field.

The spectral densities and corresponding T_1 and T_2 values, Eqs. 1a, 1b, have an angular dependence. The relaxation times are shortest at one half of the tetrahedral angle, i.e. the magic angle ($\beta_{\text{CL}} = \text{ArcCos}[-1/3]/2$) and $\alpha_{\text{CL}} = 0$, and longest at the parallel edges ($\beta_{\text{CL}} = 0$, independent of α_{CL}). For η values ≤ 0.1 , the variation of the T_1 with respect to the powder average value is less than $\pm 25\%$. The angular dependence of the T_2 value is also less than $\pm 25\%$ if $\eta = 0.1$ or less. In the deuterium spectrum, fast tetrahedral jumps ($k_{\text{tet}} > \text{qcc}$) yield a dynamically reduced powder lineshape that is a sharp, apparently isotropic, peak. Any effects of the angular dependence show up as a deviation from monoexponentiality of the relaxation of this peak.

2.4. Spectral densities and powder lineshapes for C_2 symmetry jumps

Using the appropriate correlation functions and jump matrix, we find the C_2 jump spectral densities in the *laboratory* reference frame:

$$J_0^{C_2} = \frac{1}{48k_{C_2}} ((3 + \eta)^2 (1 + \cos[\alpha]^2 \cos[4\beta] + \cos[2\beta] \sin[\alpha]^2) \sin[2\theta]^2) \quad (4a)$$

$$J_1^{C_2} = \frac{(3 + \eta)^2 (1 + \cos[\alpha]^2 \cos[4\beta] + \cos[2\beta] \sin[\alpha]^2) \sin[2\theta]^2 k_{C_2}}{12(\omega^2 + 4k_{C_2}^2)} \quad (4b)$$

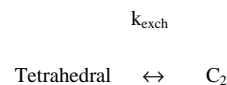
$$J_2^{C_2} = -1 \left(\frac{(3 + \eta)^2 (-3 + \cos[2\alpha] - 2 \cos[\alpha]^2 \cos[2\beta]) \sin[\beta]^2 \sin[2\theta]^2 k_{C_2}}{96(\omega^2 + k_{C_2}^2)} \right) \quad (4c)$$

where k_{C_2} is the C_2 jump rate constant in s^{-1} , θ is one half the $^2H-O-^2H$ bond angle, η is the asymmetry parameter, and $\alpha = \alpha_{CL}$ and $\beta = \beta_{CL}$ are the (powder average) Euler angles relating the crystal reference frame to the laboratory reference frame, i.e. magnetic field (we choose $\gamma_{CL} = 0$ with no loss of generality).

Fast C_2 symmetry jumps ($k_{C_2} \gg qcc$) yield a dynamically reduced deuterium powder lineshape, not an isotropic sharp line (see Fig. 1). The deuterium spectral densities and relaxation are also anisotropic. Both T_1 and T_2 relaxation times are shortest at the perpendicular edges, $\beta_{CL} = \pi/2$ and $\alpha_{CL} = \pi/2$, and longest at the parallel edges, $\beta_{CL} = 0$, $\alpha_{CL} = \pi/4$. With α_{CL} averaged, the relaxation times increase by a factor of four from the perpendicular to the parallel edges throughout the range of the C_2 jump rates k_{C_2} . The relaxation times are also very sensitive to the $^2H-O-^2H$ bond angle, with the shortest relaxation times obtained when the $^2H-O-^2H$ angle is the tetrahedral angle (i.e. $\theta_{bisector}$ is the magic angle).

2.5. Effects of exchange between tetrahedral jump and C_2 symmetry jump populations

Kanemite ($NaHSi_2O_5 \cdot 3^2H_2O$) and hydrated Na^+ -Zeolite A ($Na_{12}Al_{12}Si_{12}O_{48} \cdot 27^2H_2O$) contain water molecules that are directly coordinated to Na^+ and water molecules that are outside the direct coordination sphere of Na^+ [22,23]. Silicate and aluminosilicate surfaces provide oxygen lone pairs that serve as hydrogen bonding sites for water molecules. The combination of Na^+ and oxygen binding sites promote a solid state fixed lattice structure for water. Our hypothesis is that the $O-^2H$ bonds of water molecules directly coordinated to Na^+ experience C_2 symmetry jumps, that those of water molecules outside the direct coordination sphere of Na^+ experience tetrahedral jumps, and that there is exchange between the two populations with rate constant k_{exch} (Scheme 1): where Tetrahedral and C_2 identify the populations of water molecules experiencing tetrahedral and C_2 symmetry jumps of their O-H bond axes, respectively; and k_{exch} is the rate constant for exchange



Scheme 1.

between the populations. For convenience, we call Scheme 1 the C2TET model.

The mechanism of exchange between populations may involve transfer of intact water molecules or proton (2H) transfer between them. More complicated mechanisms are also possible. If the exchange occurs by proton transfer, it is important to recognize that O-H-O bonding is linear, and transfer of a 2H nucleus across a hydrogen bond rotates the PAS z axis of the 2H nucleus by π but does not itself affect the deuterium frequency or relaxation [11]. For the tetrahedral population, the jumps are caused by Bjerrum defects, and each deuteron is restricted to a single water molecule [6,11]. Mass transport of deuterons in this population requires Bjerrum defects and an additional mechanism such as whole molecule transport or proton transfer. For the C_2 population, the jump dynamics are also restricted to a single water molecule unless there is exchange. The details of the dynamic processes assumed in the C2TET model are under continuing investigation in our laboratories.

At high enough temperatures fast exchange between the two populations of water molecules allows for the C_2 symmetry jump powder lineshape to be further dynamically averaged by octahedral jumps. The exchange with the tetrahedral jump population provides $O-^2H$ bonds with access to all of the octahedral C_2 binding sites of the Na^+ ions, resulting in approximately octahedral jumps of the $O-^2H$ bond. This produces an isotropic single resonance rather than a C_2 jump lineshape. Furthermore, the fast exchange relaxation rate model predicts [1]:

$$(1/T_n)_{observed} = \chi_{C_2}(1/T_n)_{C_2} + \chi_{tet}(1/T_n)_{tet} \quad (5)$$

where $n = 1$ or 2 for T_1 or T_2 relaxation, χ_{C_2} = mole fraction of water molecules that are experiencing rapid C_2 symmetry jumps of their $O-^2H$ bonds, $(1/T_n)_{C_2}$ = inverse of the C_2 jump relaxation time, T_{n,C_2} , $\chi_{tet} = (1 - \chi_{C_2})$ = mole fraction of water molecules experiencing tetrahedral jumps of their $O-^2H$ bonds, and $(1/T_n)_{tet}$ = inverse of the tetrahedral jump relaxation time $T_{n,tet}$ [24].

In Figs. 2 and 3, the effects of jump rates (or rotational diffusion coefficient) and magnetic field on the powder average deuterium T_1 and T_2 values are calculated for isotropic rotational diffusion, tetrahedral jumps, C_2 symmetry jumps, and for fast exchange between water molecules experiencing C_2 symmetry jumps of their O-H bonds (assuming $\chi_{C_2} = 0.5$) with those experiencing tetrahedral jumps of their O-H bonds (assuming $\chi_{tet} = 0.5$). In both Figures it is assumed for the C2TET model that $k_{C_2}/k_{tet}(=1000)$ is constant as k_{tet} varies [25]. The assumption of fast exchange (Eq. (5)) used in the calculations does not hold at lower temperatures where $k_{exch} \leq qcc$.

The key feature is the double minimum in the theoretical T_1 dependence of the C2TET model (Fig. 2). This is caused by the difference in the dynamic frequencies k_{C_2} and k_{tet} , each of which contributes significantly to the T_1 relaxation. The dependence of the deuterium NMR relaxation times on temperature follows the dependence on jump rates, so an extended temperature range with low T_1 values may be expected in contrast to "pure" relaxation processes that have a single minimum such as isotropic rotational diffusion, C_2 symmetry jumps, or tetrahedral jumps. Of importance for experimental elucidation of the solid state, the contribution from a "slow" dynamic process, in this case the tetrahedral jumps, causes magnetic field-dependent T_1 values to be observed at higher temperatures than for "pure" relaxation processes.

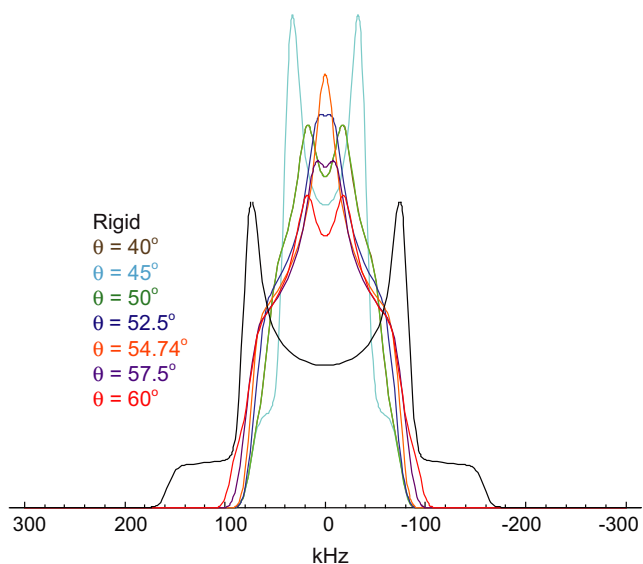


Fig. 1. Deuterium lineshapes calculated for fast ($k_{C_2} \gg qcc$) C_2 symmetry jumps and various D-O-D bond angle bisector (θ) values ($qcc = 200$ kHz, $\eta = 0$). The orange lineshape, for example, is calculated for perfectly tetrahedral D-O-D bond angles ($\theta = 54.74^\circ$, the magic angle). The two D-O-D bond angles known from the X-ray structure of water molecules coordinated to Na^+ in kanemite are 83.0° ($\theta = 41.5^\circ$) and 114.4° ($\theta = 57.2^\circ$) [22]. The overlap of spectra from $\theta = 40^\circ$ and 50° yields the forest green lineshape. All spectra, including the "rigid" powder lineshape, are calculated for $qcc = 200$ kHz, $\eta = 0$. (For interpretation of the references to color in this figure legend, the reader is referred to the web version of this paper.)

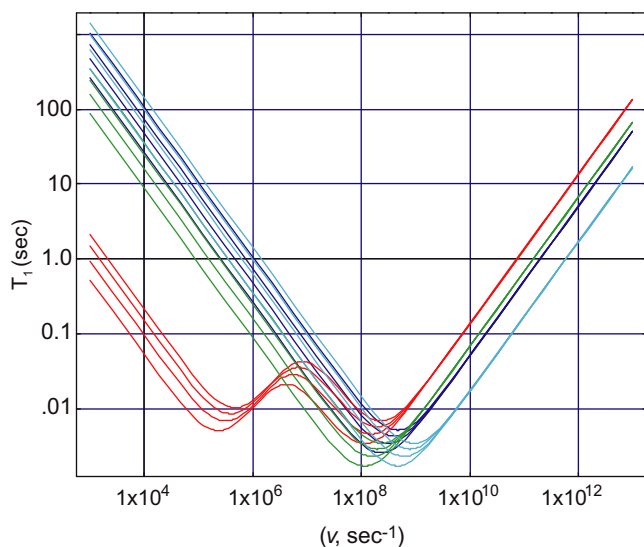


Fig. 2. Theoretical powder average deuterium T_1 values as a function of the frequency of motion, ν , calculated at four magnetic fields and corresponding Larmor frequencies: For C_2 symmetry jumps (dark blue) $\nu = k_{C_2}$, for tetrahedral jumps (green) $\nu = k_{tet}$, for isotropic rotational diffusion (light blue) $\nu = 6 D_{rot}$, and for fast exchange with equal contributions of C_2 jumps and tetrahedral jumps (red) $\nu = k_{tet}$ and $k_{C_2} = 1000 k_{tet}$ [25]. 2H quadrupolar values are $q_{cc} = 200$ kHz and $\eta = 0$. Deuterium Larmor frequencies at the four magnetic fields are 45.84 MHz, 61.42 MHz, 76.78 MHz, and 92.13 MHz. In all cases the T_1 values increase with Larmor frequency, so the lowest curve in any set corresponds to 45.84 MHz and the highest to 92.13 MHz. (For interpretation of the references to color in this figure legend, the reader is referred to the web version of this paper.)

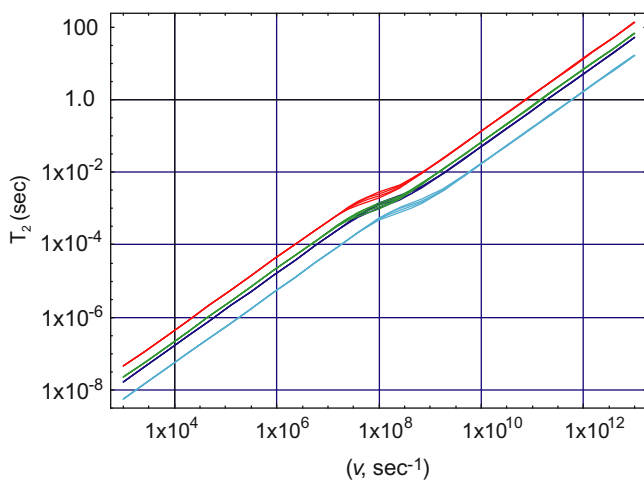


Fig. 3. Theoretical powder average deuterium T_2 values as a function of the frequency of motion, ν , calculated at four magnetic fields and corresponding Larmor frequencies: For C_2 symmetry jumps (dark blue) $\nu = k_{C_2}$, for tetrahedral jumps (green) $\nu = k_{tet}$, for isotropic rotational diffusion (light blue) $\nu = 6 D_{rot}$, and for fast exchange with equal contributions of C_2 jumps and tetrahedral jumps (red) $\nu = k_{tet}$ and $k_{C_2} = 1000 k_{tet}$ [25]. 2H quadrupolar values are $q_{cc} = 200$ kHz and $\eta = 0$. Deuterium Larmor frequencies at the four magnetic fields are 45.84, 61.42, 76.78, and 92.13 MHz. In all cases the T_2 values increase with Larmor frequency, so the lowest curve in any set corresponds to 45.84 MHz and the highest to 92.13 MHz. (For interpretation of the references to color in this figure legend, the reader is referred to the web version of this paper.)

The theoretical T_1 curves calculated for isotropic rotational diffusion in Fig. 2 are unlikely to occur experimentally under ambient conditions, since such low rotational diffusion coefficients ($6 D_{rot} \leq 10^9$ s $^{-1}$) have been observed only for supercooled liquid water at very cold temperatures and very high pressures [8].

Last, we note that the theoretical T_2 values for all models are essentially field independent.

3. Experimental

3.1. Materials

Kanemite ($NaHSi_2O_5 \cdot 3^2H_2O$), a simple phyllosilicate, was synthesized by adding 2H_2O (NMR) or 1H_2O (IR) to a mixture of δ - $Na_2Si_2O_5$ and silica gel (SiO_2) as described previously [1]. Powder X-ray analysis verified the structure of kanemite, although the presence of some amorphous material was also indicated. All samples were sealed. The weights of all samples were monitored and remained constant. Samples were stored at 21 ± 1 °C in the tightly controlled environment of the NMR Facility.

Phase pure hydrated Zeolite A ($Na_{12}Al_{12}Si_{12}O_{48} \cdot 27H_2O$), was purchased from Aldrich Chemical Co. The phase pure Zeolite A was heated at 550 °C for at least 2 h to completely remove its waters of hydration. Samples were then rehydrated by equilibrating them with H_2O vapor (FT-IR) or 2H_2O vapor (NMR) in an environmental chamber. The ratio of 2H_2O to dehydrated Zeolite A in the rehydrated samples was determined gravimetrically to be within 1% of the stoichiometric loading of 27 mol of 2H_2O per mole of Zeolite A. All samples were sealed, and their weights remained constant throughout the experiments.

3.2. X-ray crystallography and previous NMR results

The single crystal X-ray crystallography of kanemite shows fixed electron density for half of the water hydrogen atoms, specifically those that are octahedrally coordinated to Na^+ [22]. The positions of the other water hydrogen atoms in kanemite and of all of the water hydrogen atoms in hydrated Na^+ -Zeolite A are not resolvable with X-ray crystallography [22,23]. The interlayer spacing between adjacent silicate layers in kanemite is 1.03 nm [22]. The nearly spherical pore diameters in Zeolite A are 1.43 and 0.99 nm, and the approximately cylindrical channels connecting the pores have diameters of about 0.33 nm [23]. For comparison, the effective diameter of a water molecule is 0.28 nm and the diameter of a Na^+ ion is 0.19 nm [26]. X-ray crystallography and ^{23}Na solid state NMR of kanemite both show one Na^+ -binding site [22,27], but NMR studies of Zeolite A have shown variation in the location and coordination of Na^+ ions [28].

3.3. NMR measurements

2H NMR experiments were carried out over a range of temperatures at various magnetic fields, specifically 6.98, 7.01, 7.05, 7.11, 9.41, 11.73, 11.75, and 14.099 T on eight different NMR spectrometers: a solid state Chemagnetics CMX-300, two different liquid state Bruker DPX-300s, a home-built solid state spectrometer, a liquid state Bruker DRX-400, a solid state Chemagnetics/Varian Infinity 500, a liquid state Bruker AMX-2-500, and a liquid state Bruker DRX-600 spectrometer, respectively, at a range of carefully calibrated temperatures (± 1 °C).

The quadrupole echo pulse sequence, $(\pi/2)_x - \tau_1 - (\pi/2)_{xy} - \tau_2 - Acquire_x$ with Cyclops phase cycling added to all pulse phases and the receiver phase, was used to obtain 2H spectra on the solid state CMX-300 and Infinity 500 spectrometers at 45.65 and 76.77 MHz, respectively ($\pi/2 = 1.9$ – 2.5 μ s, $\tau_1 = 35$ μ s, $\tau_2 = 27$ μ s, spectral width = 2 MHz). The T_1 value of the sharp central aqueous peak was determined at various magnetic fields as a function of temperature with the inversion recovery pulse sequence, $\pi_x - \tau_{variable} - (\pi/2)_{\phi 1} - Acquire_{\phi ref}$, with $\phi 1 = x, y, -x, -y$ and $\phi ref = x, y, -x, -y$, the inversion recovery quadrupole echo experiment, $\pi_x - \tau_{variable} - (\pi/2)_x - \tau_1 - (\pi/2)_{xy} - \tau_2 - Acquire_x$ (with Cyclops), or the saturation recovery quadrupole echo experiment $[(\pi/2)_x - \tau]_n - \tau_{variable} - (\pi/2)_x - \tau_1 - (\pi/2)_{xy} - \tau_2 - Acquire_x$ (with Cyclops). The T_2 value of the sharp central peak

was determined either from the peak width at half height for fully relaxed T_1 spectra or with one of the following pulse sequences: 1. the CPMG single echo experiment: $(\pi/2)_x-\tau_{\text{variable}}-\pi_{xy}-\tau_{\text{variable}}-\text{Acquire}_x$ (with Cyclops); or 2. the CPMG double echo experiment: $(\pi/2)_x-\tau_{\text{variable}}-\pi_{xy}-2\tau_{\text{variable}}-\pi_{-y}-\tau_{\text{variable}}-\text{Acquire}_x$ (with Cyclops). At temperatures where the central peak is sufficiently sharp, $\Delta\nu_{1/2} < 3$ kHz, the data from liquid state spectrometers was obtained using “soft” pulses on the lock channel of a liquid state probe with $\pi/2 \approx 90 \mu\text{s}$ and $\pi \approx 180 \mu\text{s}$. As verified by separate experiments with hard pulses ($\pi/2 \leq 3.0 \mu\text{s}$) on the solid state CMX-300 and Infinity-500 spectrometers, this was adequate for uniform excitation of the sharp central peak at temperatures where it could be resolved. At lower temperatures where the sharp central peak could no longer be excited with soft pulses, the T_1 values were determined with $\pi/2$ pulse widths of $3 \mu\text{s}$ or less either with the inversion recovery pulse sequence, the inversion recovery quadrupole echo pulse sequence, or the saturation recovery quadrupole echo pulse sequence. For kanemite, very low temperature T_1 data were acquired at 46.46 MHz by using the saturation recovery quadrupole echo pulse sequence and monitoring the relaxation of the echo maximum [29]. Low temperature quadrupole echo spectra were obtained on solid state CMX-300 and Infinity 500 spectrometers using a Chemagnetics variable temperature apparatus. The temperature was calibrated with a copper constantan thermocouple taped in place inside the empty sample coil of the intact probe/variable temperature apparatus operating inside the magnet. The temperatures reported on these instruments are accurate to ca. ± 3 K down to 123 K.

Single pulse excitation ^{29}Si , ^{27}Al , and ^{23}Na MAS spectra for $^2\text{H}_2\text{O}$ -synthesized kanemite and $^2\text{H}_2\text{O}$ -hydrated Zeolite A were obtained at room temperature on the solid state CMX-300 and Infinity 500 spectrometers.

Theoretical ^2H NMR calculations were carried out with Mathematica[®] programs developed by the authors. These programs are available on request.

4. Results and discussion

4.1. Infrared spectroscopy

The infrared absorption spectrum of kanemite synthesized with $^1\text{H}_2\text{O}$ is presented in Fig. 4. The O– ^2H stretching region of the $^2\text{H}_2\text{O}$ -synthesized kanemite spectrum is also included and the corresponding frequencies have been multiplied by 1.36 to account for the deuterium isotope effect. Overlap observed in the O– ^1H and O– ^2H regions of these spectra clearly show broad absorption peaks between 2200 and 3700 cm^{-1} due to O–H(D) vibration in kanemite. The lattice vibration peaks in the 700–1200 cm^{-1} range do not show any H/D exchange effect or isotope effect. Five distinct broad peaks appear in the O–H(D) stretching region. These broad peaks occur around ~ 3620 , ~ 3360 , ~ 2995 , ~ 2620 , and ~ 2225 cm^{-1} . The 3620 cm^{-1} peak might be attributed to free silanol groups. Other peaks are due to the strong perturbation of the O–H(D) stretching vibration inside of the kanemite crystal structure, likely due to strong hydrogen bonding and coordination to the Na^+ ion. These broad vibrational peaks for hydroxyl groups are commonly observed for kanemite [30], but their origin is not well understood. In any case, these IR spectra clearly indicate that water in kanemite is much different than bulk water or ice, with low O–H bond stretching frequencies that are consistent with the solid state. The multiple peaks are consistent with the multiple forms of O–H expected from the crystal structure, where the electron densities for silanol (Si–O–H) hydrogens and the O–H hydrogens of the water molecules directly coordinated to Na^+ are resolved, and at least two other types of water have been proposed

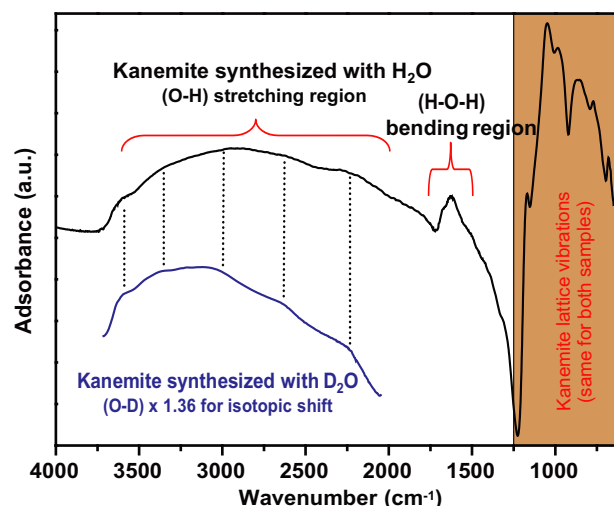


Fig. 4. Infrared Fourier transform spectrum of the water stretching region for H_2O -synthesized and D_2O -synthesized kanemite.

[22,27]. Further detailed information must be obtained from the NMR analysis.

The infrared absorption spectrum of Zeolite A as a function of time of hydration with $^1\text{H}_2\text{O}$ is shown in Fig. 5. An approximately 200 μm thick pellet of dry Zeolite A was placed inside a fully enclosed home-built environmental infrared (IR) cell with AMTIR windows. Transmission spectra were collected using a Thermo-Nicolet Nexus 670 spectrometer and a MCT detector. The system was kept at room temperature and water vapour from a liquid water reservoir was allowed to enter the environmental IR-cell. Spectra were collected approximately every 100 min following the addition of water vapour to the system. The hydrated sample spectra were divided by the background spectrum from the dry Zeolite A. The growth of the OH stretching vibration peak of water molecules absorbed in the Zeolite A was monitored as a function of time in the wavenumber region from 3000 to 3600 cm^{-1} .

Upon exposure to the near saturation vapor pressure of water, the IR peak corresponding to the absorbed water increased fast

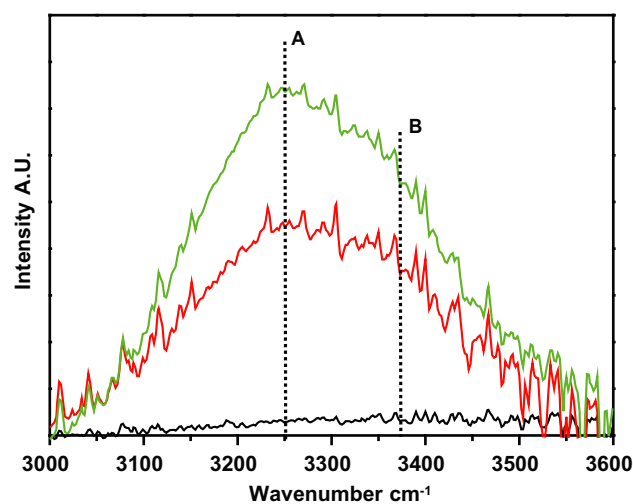


Fig. 5. Infrared absorption spectra of the water OH stretching region for water adsorption in Zeolite A are illustrated as a function of time (0, 210, and 520 min— from bottom to top). Two broad primary peaks exist around (A) 3230 cm^{-1} (by deconvolution) and (B) 3360 cm^{-1} (by deconvolution) corresponding to completely hydrogen-bonded ice-like water and water coordinated to Na^+ , respectively [31].

in the first 300 min and grew slowly thereafter. After approximately 600 min, the peak intensity did not grow significantly, indicating that the Zeolite A was almost fully saturated with water. The primary IR peak of the absorbed water in the Zeolite A is approximately 3230 cm^{-1} which is equivalent to that observed for fully hydrogen-bonded “ice-like” water [3]. It is well known that the IR adsorption band of pure liquid water is primarily made up of a broad peak around 3400 cm^{-1} . As the number of hydrogen bonds in water increases, this peak shifts to lower wavenumbers. In ice I_h , which is completely hydrogen bonded, the peak appears near 3200 cm^{-1} . The shoulder peak near 3360 cm^{-1} can be attributed to either defects in the ice-like water network inside the Zeolite pores or water coordinated around the sodium ion in the Zeolite structure. The peak for the water O–H stretching band for the first hydration layer of Na^+ in liquid solutions appears at $\sim 3423\text{ cm}^{-1}$, suggesting that the peak at 3360 cm^{-1} is from Na^+ -coordinated water [31]. The apparent simplicity of the hydrated Zeolite A IR spectrum in comparison to that of hydrated kanemite is not fully understood and will be investigated in future work.

Overall, the FT-IR data show that the water in both materials is not bulk liquid water but is more indicative of a substantially hydrogen bonded network of water coordinated to ions.

4.2. NMR results

The ^{29}Si MAS spectrum of $^2\text{H}_2\text{O}$ -synthesized kanemite is shown in Fig. 6. It shows, in addition to the main Q^3 kanemite peak at -97 ppm , about 12% Q^4 and Q^2 impurities (by deconvolution). These are consistent with the intensity of the amorphous hump in the X-ray powder spectrum.

The ^{27}Al MAS ($\nu_{\text{rot}} = 10\text{ kHz}$) NMR spectrum of $^2\text{H}_2\text{O}$ -hydrated Zeolite A is shown in Fig. 7. It shows the main tetrahedral peak, no octahedral or 5-coordinate aluminium sites, and almost no impurities.

The ^{23}Na MAS ($\nu_{\text{rot}} = 10\text{ kHz}$) spectrum of $^2\text{H}_2\text{O}$ -synthesized kanemite (Fig. 8a) shows a slightly broadened second order quadrupolar lineshape.

Nutation spectra (not shown) verify that only the central transition was excited, which is consistent with the solid state.

The ^{23}Na MAS spectrum of $^2\text{H}_2\text{O}$ -hydrated Zeolite A (Fig. 8b) shows a partially averaged second order quadrupolar lineshape, suggesting that sodium exchanges between several binding sites. The exchange is fast compared to the second order quadrupolar powder linewidth ($\sim 2.5\text{ kHz}$), but slow compared to the ^{23}Na qcc ($\sim 2.5\text{ MHz}$). The nutation spectra (not shown) verify that the central transition was selectively excited, again consistent with the solid state.

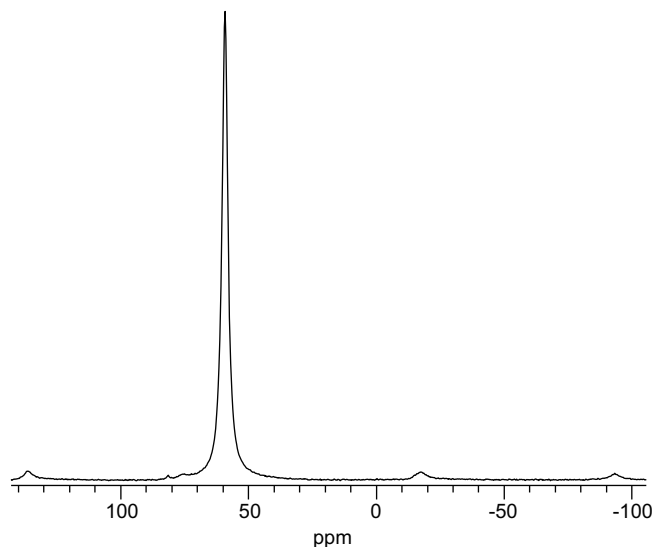


Fig. 7. ^{27}Al MAS ($\nu_{\text{rot}} = 10\text{ kHz}$) NMR spectrum of $^2\text{H}_2\text{O}$ -hydrated Zeolite A at 130.26 MHz . ($\text{pw} = 1\ \mu\text{s}$, $\text{sw} = 40\text{ kHz}$, $\text{relaxation delay} = 2\text{ s}$, $\text{ns} = 960$, $\text{td} = 1\text{ k}$). $1\text{ M AlCl}_3(\text{aq})$ (0 ppm) was as used as a secondary reference.

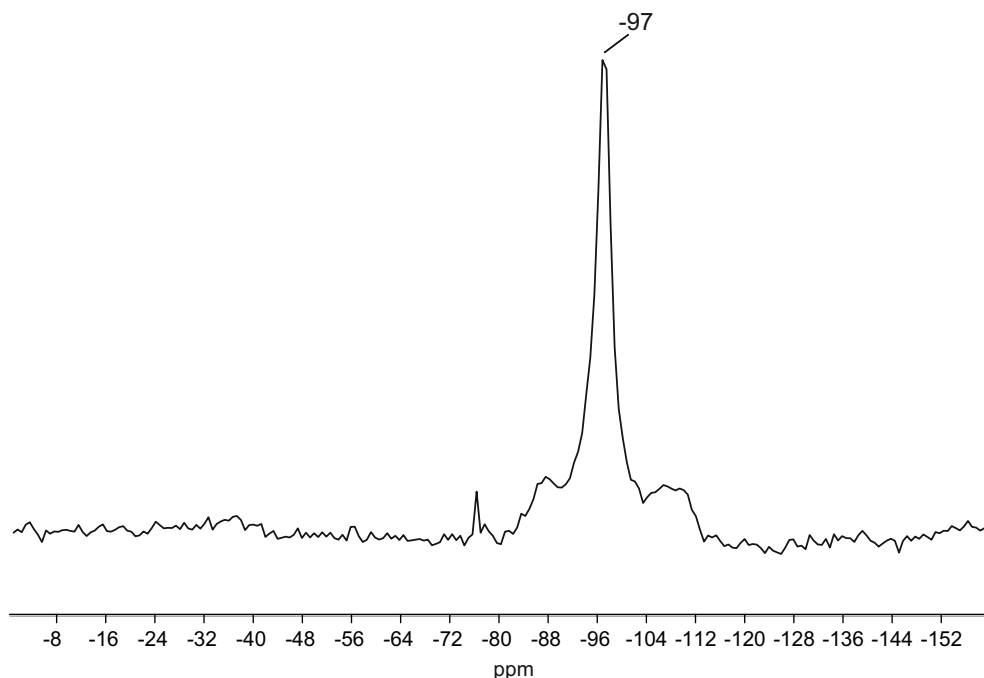


Fig. 6. Single pulse excitation ^{29}Si MAS ($\nu_{\text{rot}} = 3.5\text{ kHz}$) NMR spectrum of $^2\text{H}_2\text{O}$ -synthesized kanemite at 59.08 MHz ($\text{pw} = 6\ \mu\text{s}$, $\text{sw} = 40\text{ kHz}$, $\text{pd} = 180\text{ s}$, 476 transients , $\text{al} = 1\text{ k}$). Tetrakis(trimethylsilyl)silane was used as a secondary reference. A glitch at -76 ppm is also present in the spectrum of an empty rotor.

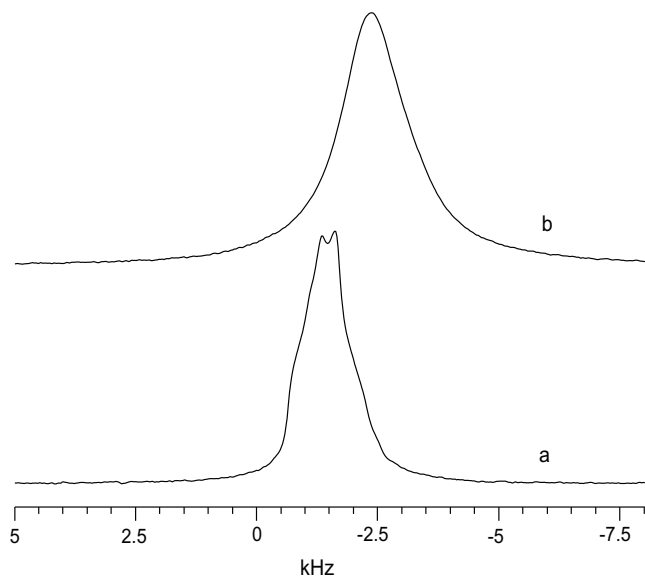


Fig. 8. (a) ^{23}Na MAS single pulse spectrum of $^2\text{H}_2\text{O}$ -synthesized kanemite at 132.16 MHz (spinrate = 10 kHz, pw = 1 μs , sw = 50 kHz, pd = 1 s, 3072 transients, al=1 k). (b) ^{23}Na MAS single pulse spectrum of $^2\text{H}_2\text{O}$ -hydrated Zeolite A at 132.16 MHz (spinrate = 10 kHz, pw = 1 μs , sw = 50 kHz, pd = 1 s, 3424 transients, al = 1k).

4.3. Theoretical intermediate exchange ^2H NMR spectra

Theoretical intermediate exchange powder lineshapes as a function of the *tetrahedral* jump rate k_{tet} are shown in Fig. 9. The method described by Vega and Luz was used to calculate interme-

mediate exchange quadrupole echo time domain signals [32]. Effects of motion during the τ delays of the quadrupole echo experiment were included in the calculations of the time domain signals. The spectra were obtained by Fourier transformation of the calculated time domain signals. The echo intensities for tetrahedral jumps in the intermediate exchange regime are severely attenuated in the range $10^4 \text{ s}^{-1} \leq k_{\text{tet}} \leq 10^6 \text{ s}^{-1}$. If the C2TET model holds, this would be expected to be manifested in the experimental quadrupole echo data.

Theoretical intermediate exchange powder lineshapes as a function of the C_2 jump rate k_{C_2} are shown in Fig. 10. Unlike the tetrahedral jump quadrupole echo intensity, the C_2 jump quadrupole echo intensity does not fall below 12% of its maximum value.

Quadrupole echo intensities for octahedral jumps have been calculated as a function of the octahedral jump rate ν in Fig. 11. Consideration of the octahedral jump rate is necessary with the C2TET model because exchange between the O^{2-}H populations experiencing C_2 symmetry jumps and tetrahedral jumps generates approximately *octahedral* jumps of O^{2-}H bond vectors as they sample the different water binding sites of the Na^+ ions. We assume that the exchange process is rate limiting, so the C2TET kinetic parameter k_{exch} can be identified with the octahedral jump rate. For $10^4 \text{ s}^{-1} \leq k_{\text{exch}} \leq 10^6 \text{ s}^{-1}$, the quadrupole echo intensity for octahedral jumps nearly vanishes. If the C2TET model holds, the corresponding loss of echo intensity would be expected in the experimental data.

4.4. Experimental low temperature ^2H NMR spectra

Zeolite A contains no silanol groups, so the low temperature ^2H powder spectra of $^2\text{H}_2\text{O}$ -hydrated Zeolite A are simpler than those of kanemite. The experimental quadrupole echo spectra of $^2\text{H}_2\text{O}$ -hydrated Zeolite A are shown in Fig. 12. with theoretical simula-

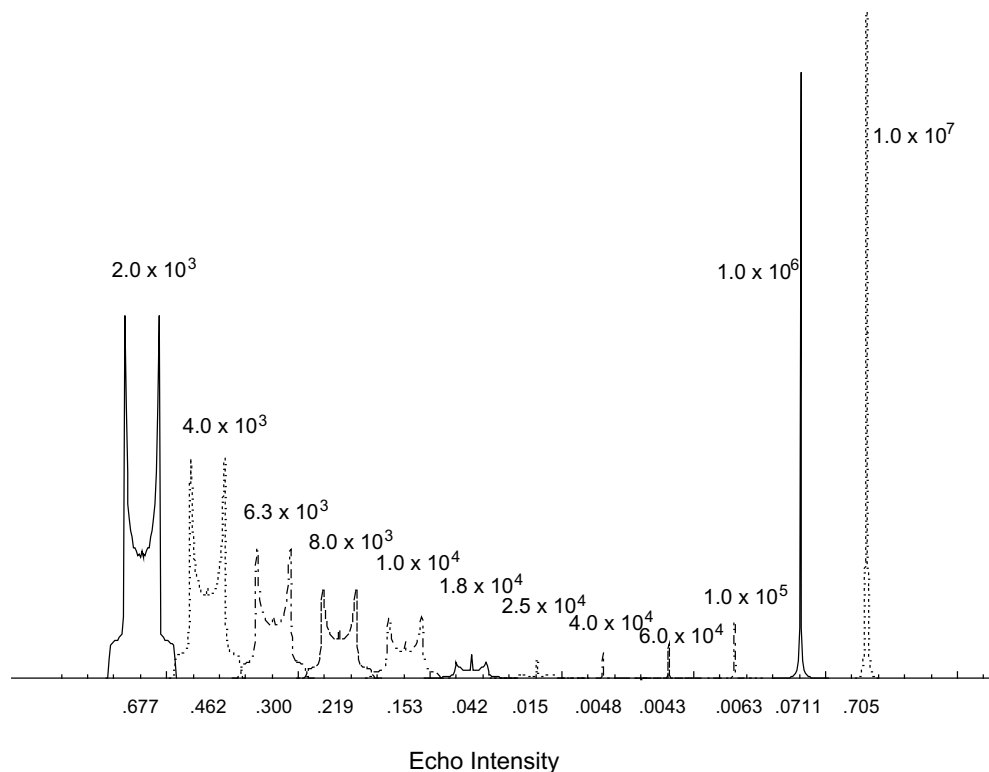


Fig. 9. Deuterium powder lineshapes calculated for tetrahedral jumps of the O^{2-}H bond as a function of the tetrahedral jump rate k_{tet} . The k_{tet} values are shown on top of the corresponding lineshapes, and the echo intensities are shown underneath the corresponding lineshapes. The isotropic peaks at the highest jump rates have been truncated to fit on scale. The following parameters were used: $q_{\text{cc}} = 200 \text{ kHz}$, $\eta = 0$, $\tau = 35 \mu\text{s}$ (echo delay in quadrupole echo experiment).

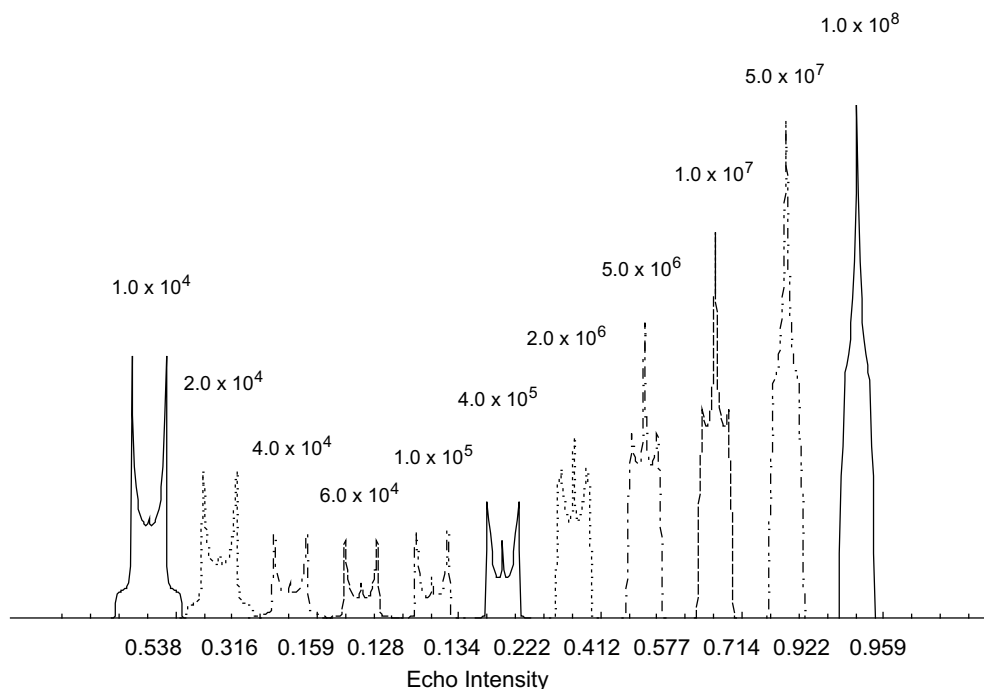


Fig. 10. Deuterium powder lineshapes calculated for C_2 symmetry jumps of the $O-^2H$ bond as a function of the jump rate k_{C_2} . The k_{C_2} values are shown on top of the corresponding lineshapes, and the echo intensities are shown underneath the corresponding lineshapes. The following parameters were used: $qcc = 200$ kHz, $\eta = 0$, $\tau = 35$ μ s (echo delay in quadrupole echo experiment), and an equally weighted mixture (0.5 weight each) of $\theta = 52.5^\circ$ and $\theta = \text{magic angle}$.

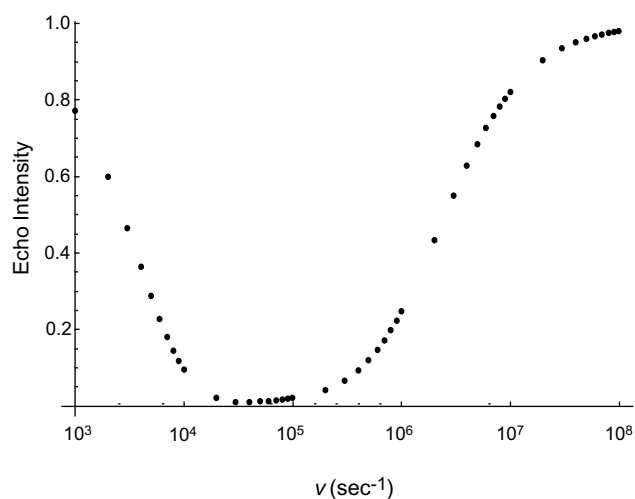


Fig. 11. Deuterium powder echo intensities calculated for octahedral symmetry jumps of the $O-^2H$ bond as a function of the jump rate $\nu = k_{\text{exch}}$. The following parameters were used: $qcc = 200$ kHz, $\eta = 0$, $\tau = 35$ μ s (echo delay in quadrupole echo experiment).

tions. At the lowest temperature we could maintain, 141 K, the quadrupole echo spectrum is consistent with the rigid deuterium powder spectrum of 2H_2O with $\nu_{\text{motion}} \ll qcc$, $qcc \approx 200$ kHz, and $0 \leq \eta \leq 0.1$, Table 1. At 203 and 210 K, the spectra are consistent with a combination of nearly rigid 2H_2O and a lineshape close to that calculated for C_2 symmetry jumps with $k_{C_2} > qcc$. We therefore assign the “rigid” parts of these spectra to the population of $O-^2H$ bonds experiencing tetrahedral jumps with $k_{\text{tet}} \ll qcc$. The resolvability of both deuterium populations, C_2 and tetrahedral, also shows that $k_{\text{exch}} \ll qcc$. At 222 and 232 K, the rigid deuterium powder pattern is not resolvable, but the C_2 symmetry jump powder lineshape is still observable. This is consistent with the loss of intensity

for tetrahedral jumps as they approach the intermediate exchange regime, $k_{\text{tet}} \sim qcc$, (Fig. 9). The extremely low experimental quadrupole echo intensities and limited resolvability of the remaining C_2 symmetry jump lineshapes, suggests further that k_{exch} approaches qcc at these temperatures, consistent with octahedral jumps in intermediate exchange and the C2TET model. The theoretical echo intensities in Fig. 12 do not include the effects of octahedral jumps. The simultaneity of the decrease in k_{tet} and k_{exch} suggests that the exchange process may require tetrahedral jumps. Above 251 K the quadrupole echo spectra show a single apparently isotropic peak. This is consistent with the C2TET model if $k_{\text{exch}} > qcc$ and $k_{C_2} \gg qcc$.

Eyring plots [33] of the temperature dependent rate constants are shown in Fig. 13, where the estimated values of k_{C_2} and k_{tet} from Fig. 12 have been used. For the hydrated Zeolite A, the kinetic activation parameters for the tetrahedral and C_2 symmetry jumps are $\Delta H_{\text{tet}}^\ddagger = +17$ kJ/mol, $\Delta S_{\text{tet}}^\ddagger = -111$ J/(mol K), $\Delta H_{C_2}^\ddagger = +20$ kJ/mol, and $\Delta S_{C_2}^\ddagger = -15$ J/(mol K).

The variable temperature quadrupole echo 2H spectra of 2H_2O -synthesized kanemite are complicated by the presence of a silanol ($Si-O-^2H$) powder pattern with a notable downfield silanol chemical shift [2] that persists throughout the temperature range, Fig. 14. At the lowest temperature we could maintain, 132 K, the broad powder pattern of rigid 2H_2O ($k_{C_2} < qcc$, $k_{\text{tet}} \ll qcc$, Table 1) is dominant, but the narrower silanol powder pattern is still apparent. At 218 K, there is still a rigid powder pattern that we assign to $O-^2H$ bonds experiencing tetrahedral jumps ($k_{\text{tet}} \ll qcc$), a silanol powder pattern, and also a central bump that we assign to $O-^2H$ bonds experiencing C_2 symmetry jumps ($k_{C_2} \sim qcc$). At 256 K, the rigid powder pattern has disappeared and the spectrum is a combination of the silanol powder pattern and a powder pattern that we assign to fast C_2 symmetry jumps ($k_{C_2} \gg qcc$). A powder lineshape from $O-^2H$ bonds experiencing tetrahedral jumps is no longer observable, suggesting that k_{tet} approaches qcc with correspondingly low intensity, Fig. 9. At 275 K, the spectrum is a sum of the silanol powder pattern and an intense central peak. The cen-

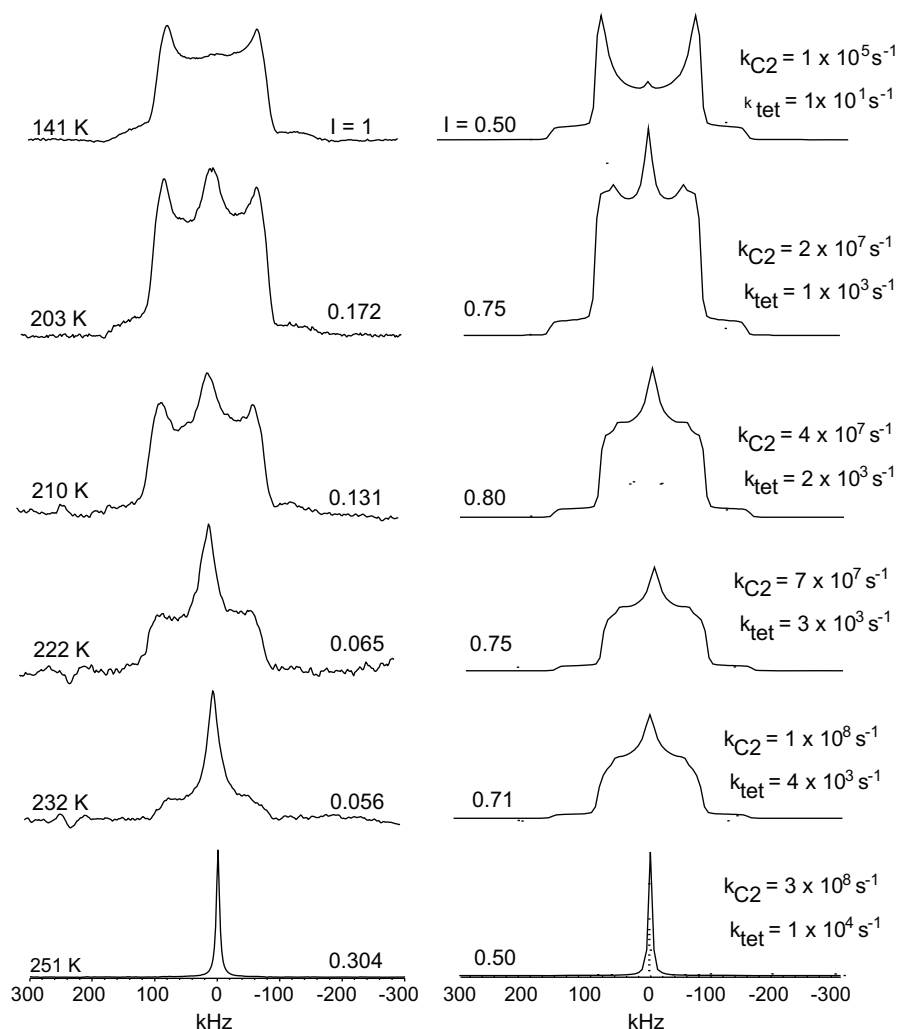


Fig. 12. Experimental (left) and simulated (right) variable temperature quadrupole echo spectra of $^2\text{H}_2\text{O}$ -hydrated Zeolite A. The quadrupole echo pulse sequence $((\pi/2)_x - \tau_1 - (\pi/2)_{xy} - \tau_2 - \text{acquire}_x$ with Cyclops phase cycling added to all pulse phases and the receiver phase) was used to obtain ^2H spectra on the solid state Infinity 500 spectrometer at 76.77 MHz ($\pi/2 = 2.0 \mu\text{s}$, $\tau_1 = 35 \mu\text{s}$, $\tau_2 = 27 \mu\text{s}$, spectral width 2 MHz). Approximate theoretical spectra and echo intensities were calculated assuming equal contributions from deuterium populations experiencing C_2 symmetry jumps of their O- ^2H bonds and tetrahedral jumps of their O- ^2H bonds, each with $q_{cc} = 200 \text{ kHz}$, $\eta = 0$. The C_2 population was further subdivided into two equal populations with $\theta = \text{magic angle}$ and $\theta = 52.5^\circ$. The theoretical spectrum for 251 K was simulated by assuming that the C_2 symmetry jumps had been isotropically averaged by octahedral exchange between different C_2 binding sites.

Table 1

Summary of the estimates of C2TET rate constants relative to the O- ^2H quadrupole coupling constant (q_{cc})

Substance	T (K)	k_{C_2}	k_{tet}	k_{exch}^a	Other comments
Zeolite A	141	$\ll q_{cc}$	$\ll\ll q_{cc}$	$\ll\ll q_{cc}$	
Hydrated	203–210	$\gg q_{cc}$	$\ll\ll q_{cc}$	$\ll\ll q_{cc}$	
With D_2O	222–232	$\gg q_{cc}$	$\leq q_{cc}$	$\leq q_{cc}$	
	>251	$\gg q_{cc}$	$\sim q_{cc}$	$> q_{cc}$	
Kanemite	132	$\ll q_{cc}$	$\ll\ll q_{cc}$	$\ll\ll q_{cc}$	DSP ^b
Synthesized	218	$\sim q_{cc}$	$\ll q_{cc}$	$\ll q_{cc}$	DSP
With D_2O	256	$\gg q_{cc}$	$\leq q_{cc}$	$\leq q_{cc}$	DSP
	275	$\gg q_{cc}$	$\sim q_{cc}$	$\geq q_{cc}$	DSP
	296	$\gg q_{cc}$	$> q_{cc}$	$\gg q_{cc}$	DSP

^a There is greater uncertainty in k_{exch} estimates.

^b A dynamic silanol pattern (DSP) persists throughout the temperature range.

tral peak retains some features characteristic of the fast exchange C_2 jump lineshape, suggesting that $k_{exch} \sim q_{cc}$. At 296 K, the central peak has narrowed, suggesting that $k_{exch} \gg q_{cc}$. Unlike the case for $^2\text{H}_2\text{O}$ -hydrated Zeolite A, there is *not* a huge loss of experimental echo intensity at temperatures where k_{tet} and k_{exch} are in interme-

diated exchange. This is consistent with a non-vanishing contribution from the silanol O- ^2H . The presence of the silanol powder lineshape shows that the silanol deuterium nuclei are not exchanging rapidly with water deuterium nuclei. Further studies of the low temperature silanol, tetrahedral and C_2 symmetry dynamics in kanemite are underway.

4.5. Field dependent variable temperature ^2H relaxation data for the sharp central resonance of the kanemite and Zeolite A samples

The T_1 data obtained for the sharp water peak at temperatures where it could be resolved and inverted with soft pulses, above $\sim 252 \text{ K}$ for $^2\text{H}_2\text{O}$ -hydrated Zeolite A, and above 279 K for $^2\text{H}_2\text{O}$ -synthesized kanemite, were monoexponential. When fit with the Kohlrausch stretched exponential function, the T_1 relaxation data obtained for the sharp central peaks of both samples yield $\beta > .94$ in all cases with the lowest β values obtained at the lowest temperatures, consistent with monoexponential relaxation or a narrow range of relaxation times [34]. At lower temperatures the intermediate exchange powder lineshapes emerge and prevent direct determination of T_1 values for the sharp central peak.

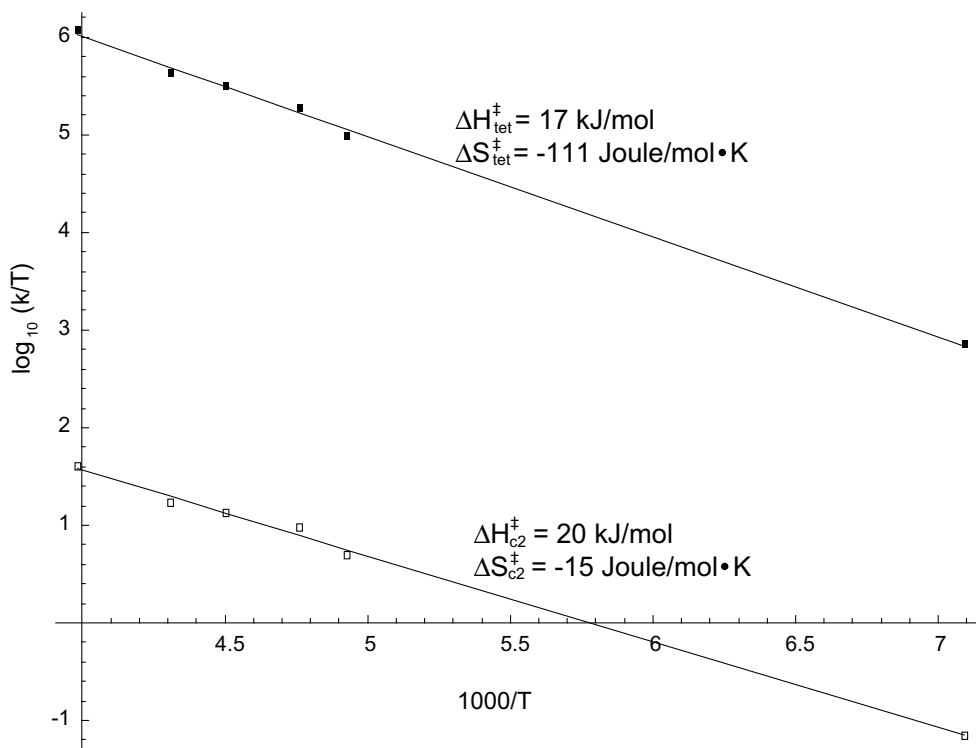


Fig. 13. Eyring plots [33] of the k_{C_2} and k_{tet} values in $^2\text{H}_2\text{O}$ -hydrated Zeolite A obtained from the simulations in Fig. 12. The activation parameters are $\Delta H_{tet}^\ddagger = +17$ kJ/mol, $\Delta S_{tet}^\ddagger = -111$ J/(mol K), $\Delta H_{C_2}^\ddagger = +20$ kJ/mol, and $\Delta S_{C_2}^\ddagger = -15$ J/(mol K).

Low temperature T_1 data for $^2\text{H}_2\text{O}$ -synthesized kanemite (we have not yet run these experiments for $^2\text{H}_2\text{O}$ -hydrated Zeolite A) were obtained at 46.46 MHz from the full echo intensity in a saturation recovery quadrupole echo experiment with hard pulses. Two types of deuterium spin lattice relaxation were observed: a slowly relaxing component ($\beta \approx 0.6$) that is tentatively assigned to the silanol deuterium and a faster relaxing monoexponential component ($\beta > 0.9$) that is assigned to the O- ^2H bonds experiencing tetrahedral and C_2 symmetry jumps. At temperatures where both methods were used, 288 and 295 K, the fast relaxing component and the sharp central peak had the same T_1 values within experimental error (ca. $\pm 10\%$) at 46.46 and 46.07 MHz. The experimental T_1 and T_2 values for the sharp central peak of $^2\text{H}_2\text{O}$ -synthesized kanemite and $^2\text{H}_2\text{O}$ -hydrated Zeolite A are shown in Figs. 15 and 16, respectively.

The O- ^2H bond motions in $^2\text{H}_2\text{O}$ -synthesized kanemite and in $^2\text{H}_2\text{O}$ -hydrated Zeolite A are very different than they are in bulk liquid water. In bulk liquid $^2\text{H}_2\text{O}$ and in supercooled $^2\text{H}_2\text{O}$ at atmospheric pressure, the extreme narrowing condition is met, with $D_{rot} \gg \nu_{Larmor}$, and $T_1 = T_2$. This is not the case for $^2\text{H}_2\text{O}$ in $^2\text{H}_2\text{O}$ -synthesized kanemite or in $^2\text{H}_2\text{O}$ -hydrated Zeolite A, where the T_1 and T_2 values differ by 2.5–3 orders of magnitude. Therefore motions comparable to or slower than the Larmor frequency must occur throughout the experimental temperature range of both samples.

This is confirmed by the ^2H NMR T_1 values for both $^2\text{H}_2\text{O}$ -synthesized kanemite and $^2\text{H}_2\text{O}$ -hydrated Zeolite A, which are nearly two orders of magnitude shorter than those of bulk liquid $^2\text{H}_2\text{O}$ at the same temperatures. In addition, for both samples the T_1 values show significant magnetic field dependence that increases with temperature above 277 K. The field dependence exceeds the experimental uncertainty (ca. $\pm 10\%$) in the T_1 values at these temperatures. The minima in the experimental T_1 values occur near 284 and 267 K, respectively, for $^2\text{H}_2\text{O}$ -synthesized kanemite and

$^2\text{H}_2\text{O}$ -hydrated Zeolite A. The temperatures for these T_1 minima may be compared to the temperatures for the T_1 minima for isotropic rotational diffusion of supercooled liquid $^2\text{H}_2\text{O}$ at comparable magnetic fields, which occur at temperatures below 200 K and pressures above 2000 atm [8].

The scatter in the T_1 data obtained for $^2\text{H}_2\text{O}$ -synthesized kanemite with the saturation recovery method (black triangles) between 250 and 280 K (Fig. 15) may indicate that the tetrahedral jump rate k_{tet} and the exchange rate k_{exch} are both in the intermediate exchange region at these temperatures (see Fig. 11). Other possible explanations for the differences are under investigation.

There were significant differences in the experimental T_2 values (76.77 MHz) determined by peak width, single echo CPMG experiments, and double echo CPMG experiments. However, the values obtained with any given experiment at any temperature were reproducible. Residual powder lineshapes for asymmetry in the tetrahedral, C_2 , or octahedral jumps may contribute to the observed peak width and reduce the linewidth-derived T_2 value. The variation of the T_2 values with the experimental method is also consistent with the effects of intermediate exchange on T_2 relaxation [36]. This hypothesis will be examined in future work. In Figs. 15 and 16, the double echo CPMG T_2 values are plotted, since these are the longest T_2 values observed. The linewidth-derived T_2 values for $^2\text{H}_2\text{O}$ -hydrated Zeolite A are also shown in Fig. 16 to illustrate the magnitude of the discrepancy between the values obtained with the different methods. T_2 values determined for a few temperatures at 46.03 MHz with each of the three methods verified magnetic field (Larmor frequency) independence for each method within experimental error (ca. $\pm 10\%$). The lack of field dependence for T_2 combined with the lack of consistent values from different experimental methods makes the experimental T_2 dependence on temperature less reliable for comparison with theory than the T_1 dependence.

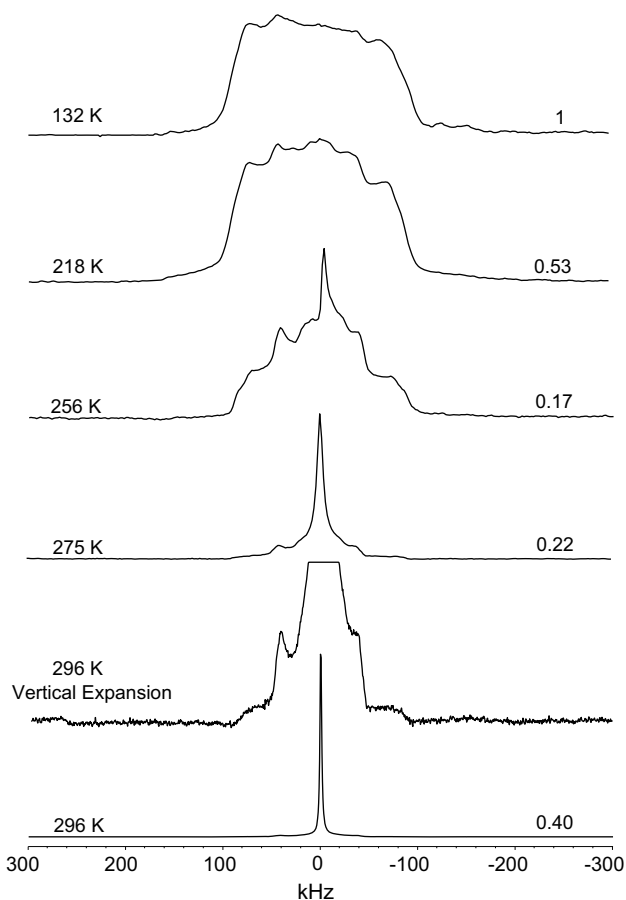


Fig. 14. Experimental variable temperature quadrupole echo spectra of $^2\text{H}_2\text{O}$ -synthesized kanemite. The quadrupole echo pulse sequence was used on the solid state Infinity 500 spectrometer at 76.77 MHz ($\pi/2 = 2.0\mu\text{s}$, $\tau_1 = 35\mu\text{s}$, $\tau_2 = 27\mu\text{s}$, spectral width 2 MHz). Experimental echo intensities relative to the intensity at 132 K are shown on the right side of each spectrum. A vertical expansion of the spectrum at 296 K is included to show the silanol powder pattern that persists through the temperature range.

4.6. Comparison of theory and experiment for T_1 relaxation

The experimental deuterium T_1 data for the sharp central peak of $^2\text{H}_2\text{O}$ -hydrated Zeolite A obtained with “soft” pulses over a range of fixed temperatures at 46.03, 61.42, 76.77, and 92.13 MHz are plotted on the background of the best fit theoretical T_1 values for the C2TET model in Figs. 16 and 17. Experimental T_1 values obtained at the same temperature but at different magnetic fields were plotted against the theoretical curves that gave the best match, assuming that k_{C_2}/k_{tet} is constant for the C2TET model. This assumption is justified for $^2\text{H}_2\text{O}$ -hydrated Zeolite A by the similar activation enthalpies for k_{C_2} and k_{tet} calculated from the low temperature quadrupole echo spectra of Figs. 12 and 13, but we have yet to verify if this is also true for $^2\text{H}_2\text{O}$ -synthesized kanemite. Nevertheless, this is the simplest possible assumption for the C2TET model. Experimental T_1 values for bulk water are off the scale of the plot and show no magnetic field dependence. The pure tetrahedral and pure C_2 symmetry jump models can not reproduce the extended temperature range of the magnetic field dependence. The isotropic rotational diffusion model, with $\nu = 6 D_{\text{rot}}$ values characteristic of supercooled liquid water at 200 K and 2000 atm, can not match the magnetic field dependence either. Only the fast exchange C2TET model was able to reproduce the experimental data. A more complete study of the relationship between k_{C_2} and k_{tet} is

underway. We recognize that the assumption of equal activation enthalpies for k_{C_2} and k_{tet} may have to be revised.

In Fig. 18, the plot is extended to lower temperatures, where the fit obtained for the C2TET model with $k_{C_2}/k_{\text{tet}} = 25,833$ no longer matches as well. The experimental values instead approach the values expected for pure C_2 jumps. This is easily explained in the context of the C2TET model. At lower temperatures the tetrahedral jump rate falls into the intermediate exchange regime ($k_{\text{tet}} \sim \text{qcc}$) and the contribution to the deuterium NMR intensity from the tetrahedrally jumping $\text{O}-^2\text{H}$ bond population drops in comparison to that of the C_2 symmetry jumping $\text{O}-^2\text{H}$ bond population, which is still in fast exchange ($k_{C_2} \gg \text{qcc}$). The process represented by the C2TET exchange rate constant k_{exch} may also go into intermediate exchange at the same temperatures. Further details will be elucidated in future work.

In Fig. 19, we show Eyring plots [33] of the rate constants k_{C_2} and k_{tet} estimated from the C2TET model for $^2\text{H}_2\text{O}$ -hydrated Zeolite A in Fig. 17 along with the k_{C_2} and k_{tet} values estimated from the low temperature quadrupole echo spectra (Fig. 12). The best fit activation parameters for C_2 and tetrahedral jumps are $\Delta H_{\text{tet}}^\ddagger = +17\text{ kJ/mol}$, $\Delta S_{\text{tet}}^\ddagger = -109\text{ J/(mol K)}$, $\Delta H_{C_2}^\ddagger = +19\text{ kJ/mol}$, and $\Delta S_{C_2}^\ddagger = -20\text{ J/(mol K)}$, respectively, very close to the values estimated from the variable temperature quadrupole echo spectra alone. The consistency of the data obtained from the two different deuterium NMR techniques supports the C2TET model.

The experimental T_1 data obtained with “soft” pulses over a range of fixed temperatures at 46.03 and 76.77 MHz for the sharp central resonance of $^2\text{H}_2\text{O}$ -synthesized kanemite are plotted on the background of the best fit theoretical T_1 values for the C2TET model in Figs. 20 and 21. As with Zeolite A, experimental T_1 values for bulk water are off the scale, pure tetrahedral and pure C_2 symmetry jump models can not reproduce the extended temperature range of the magnetic field dependence, and isotropic rotational diffusion with $\nu = 6 D_{\text{rot}}$ values characteristic of supercooled liquid water at 200 K and 2000 atm, can not match the magnetic field dependence either. Only the C2TET model was able to reproduce the experimental data obtained at higher temperatures ($\geq 298\text{ K}$, Fig. 20). The optimal k_{C_2}/k_{tet} ratio is 1000. The fit between the experimental and best fit C2TET model is good for temperatures above 298 K, but deviates from the C2TET model at lower temperatures where the tetrahedral jump rate k_{tet} and exchange rate k_{exch} go into intermediate exchange (Figs. 9, 11). Based on the C2TET model, the experimentally observed relaxation times in this temperature region should therefore be dominated by the population of water molecules experiencing C_2 jumps. This prediction is verified in Fig. 21.

Eyring plots [33] of the calculated k_{tet} and k_{C_2} values for $^2\text{H}_2\text{O}$ -synthesized kanemite from Figs. 20 and 21 are shown in Fig. 22. The activation parameters for kanemite are $\Delta H_{\text{tet}}^\ddagger = +23\text{ kJ/mol}$, $\Delta S_{\text{tet}}^\ddagger = -69\text{ J/(mol K)}$, $\Delta H_{C_2}^\ddagger = +23\text{ kJ/mol}$, and $\Delta S_{C_2}^\ddagger = -11\text{ J/(mol K)}$.

It is apparent for both $^2\text{H}_2\text{O}$ -synthesized kanemite and $^2\text{H}_2\text{O}$ -hydrated Zeolite A that the k_{C_2} and k_{tet} jump rate values calculated from the T_1 data are consistent with the experimental low temperature quadrupole echo lineshapes. The consistency of the data is also confirmed by the lowest temperature at which the sharp central resonance can be inverted in the T_1 experiments for both samples. Numerical Bloch equation calculations for tetrahedral jumps of $\text{O}-^2\text{H}$ bonds show that soft pulses, such as those used in most of the T_1 experiments, are not able to invert the sharp central resonance obtained from tetrahedral jumps as k_{tet} falls below about $1 \times 10^6\text{ s}^{-1}$. The ability to invert the part of the sharp central resonance arising from the population of water molecules experiencing C_2 and octahedral jumps of their $\text{O}-^2\text{H}$ bonds persists to slightly lower temperatures, presumably since $k_{C_2} \gg \text{qcc}$ and $k_{\text{exch}} > \text{qcc}$. Experimentally, the loss of the ability to invert the sharp central

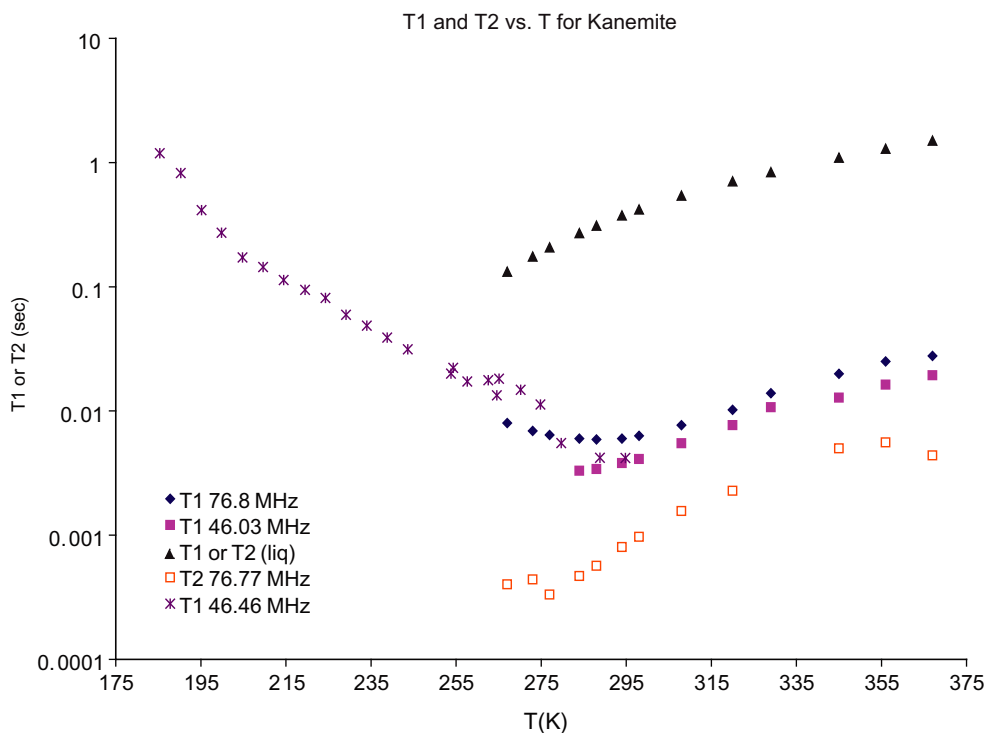


Fig. 15. The experimental deuterium T_1 data for the sharp central resonance of $^2\text{H}_2\text{O}$ -synthesized kanemite at 46.03 (purple squares) and 76.77 MHz (dark blue diamonds); T_1 data obtained at low temperature for the fast-relaxing component at 46.46 MHz (purple crosses), and T_2 data obtained with the double echo CPMG experiment at 76.77 MHz (orange squares) The temperature dependent $T_1 = T_2$ values (black triangles) for bulk $^2\text{H}_2\text{O}$ at atmospheric pressure are shown for comparison [35]. (For interpretation of the references to color in this figure legend, the reader is referred to the web version of this paper.)

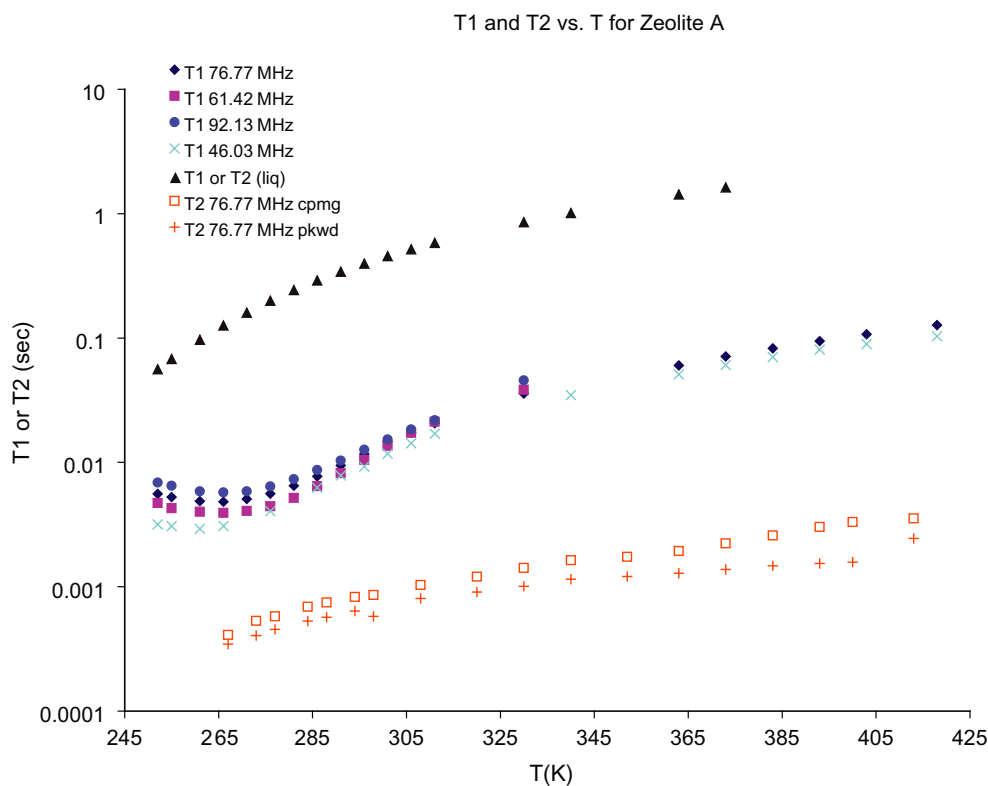


Fig. 16. The experimental deuterium T_1 data for the sharp central resonance of $^2\text{H}_2\text{O}$ -hydrated Zeolite A at 46.03 (light blue x'es), 61.42 MHz (purple squares), 76.77 MHz (dark blue diamonds), and 92.13 MHz (filled blue circles). The T_2 values at 76.77 MHz obtained with the double echo CPMG experiment (orange squares) and from the sharp peak linewidth (orange crosses) are also shown. The temperature dependent $T_1 = T_2$ values (black triangles) for bulk $^2\text{H}_2\text{O}$ at atmospheric pressure are shown for comparison [35]. (For interpretation of the references to color in this figure legend, the reader is referred to the web version of this paper.)

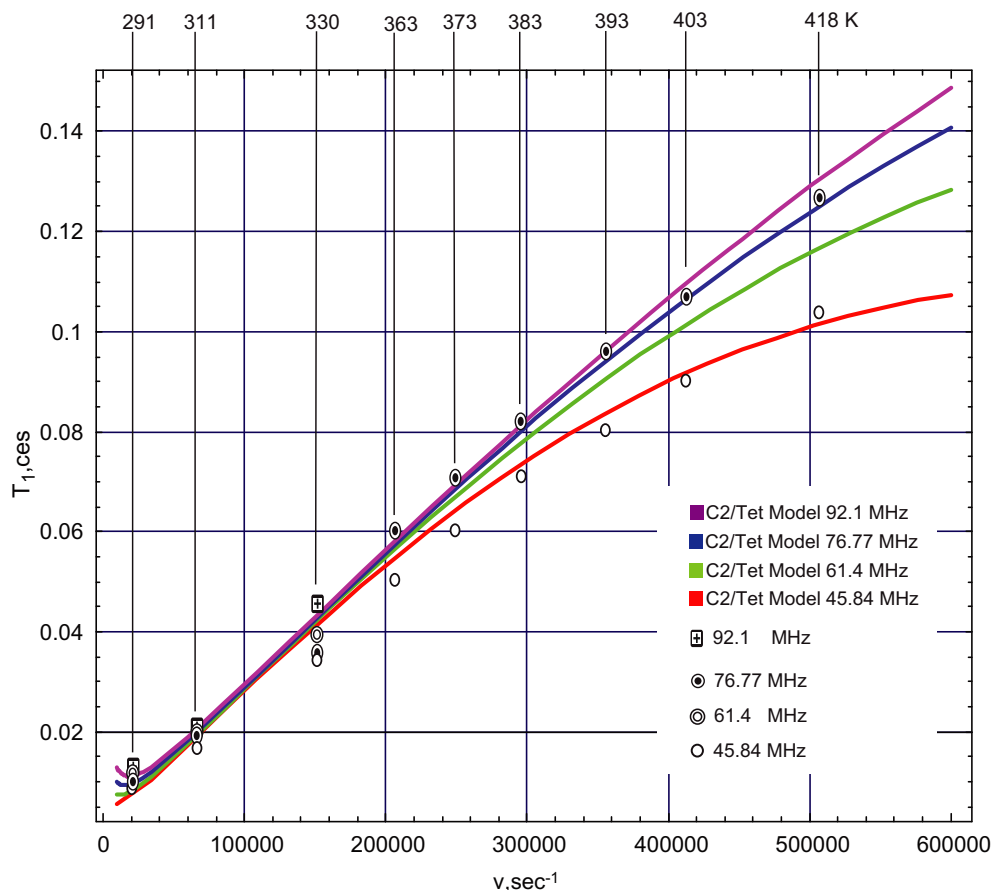


Fig. 17. The high temperature experimental T_1 data for the sharp central resonance of $^2\text{H}_2\text{O}$ -hydrated Zeolite A are plotted on the background of the best fit theoretical T_1 values for the C2TET model ($\chi_{\text{tet}} = \chi_{\text{C}_2} = 0.5$, $\nu = k_{\text{tet}}$, $k_{\text{C}_2}/k_{\text{tet}} = 25,833$) for deuterium frequencies of 46.03, 61.42, 76.77, and 92.13 MHz. The ratio of $k_{\text{C}_2}/k_{\text{tet}}$ was assumed to be constant throughout the temperature range, and was chosen to yield the best possible fit of the resulting theoretical curves to the experimental data. Curves for pure tetrahedral jumps and pure isotropic rotational diffusion are off the scale of this figure. There was no way to fit the experimental data with the isotropic rotational diffusion model or the perfect tetrahedral jump model. The best fit was obtained with $q_{\text{cc}} = 200$ kHz and $\eta = 0$.

resonance was observed at temperatures where the C2TET model predicts both k_{tet} and k_{exch} are in the intermediate exchange regime, $k_{\text{tet}} \sim q_{\text{cc}}$ and $k_{\text{exch}} \sim q_{\text{cc}}$.

4.7. Comparison of theory and experiment for T_2 relaxation

The experimental T_2 data obtained over a range of temperatures at 76.77 MHz [37] for the sharp central resonances of $^2\text{H}_2\text{O}$ -hydrated Zeolite A and $^2\text{H}_2\text{O}$ -synthesized kanemite are plotted on the background of the theoretical T_2 values calculated for isotropic rotational diffusion ($\nu = 6 D_{\text{rot}}$), ideal C_2 symmetry jumps ($\nu = k_{\text{tet}}$, $k_{\text{C}_2} = 25,833 * k_{\text{tet}}$ for Zeolite A; $\nu = k_{\text{tet}}$, $k_{\text{C}_2} = 1000 * k_{\text{tet}}$ for kanemite); ideal tetrahedral jumps ($\nu = k_{\text{tet}}$), and the C2TET model, Eq. [3,9,12–14] in Figs. 23 and 24. In these plots it was assumed for the C2TET model that $\nu = k_{\text{tet}}$ and $k_{\text{C}_2}/k_{\text{tet}} = 25,833$ for the Zeolite A data and $k_{\text{C}_2}/k_{\text{tet}} = 1000$ for the kanemite data, respectively, the same values used for the T_1 plots in Figs. 17–21.

The experimental T_2 values for both samples depend on the NMR method used to obtain them, consistent with intermediate exchange effects on the T_2 relaxation times [36]. Using the same k_{tet} and k_{C_2} values and ratios as for the T_1 analyses, the experimental data lie between the theoretical T_2 for C_2 symmetry jumps and the theoretical T_2 expected for the other models (C2TET, pure tetrahedral, or isotropic rotational diffusion). This observation is consistent with the C2TET model, because T_2 relaxation is more sensitive to exchange effects than T_1 relaxation [36], and k_{tet} is in the intermediate exchange regime (Fig. 9). As a consequence, the

contribution to the observed deuterium relaxation from the population of water molecules experiencing tetrahedral jumps of their O– ^2H bonds is severely attenuated, yielding results that are dominated by the population of water molecules experiencing C_2 symmetry jumps of their O– ^2H bonds.

5. Conclusions

It is widely recognized that a variety of models can be used to match NMR relaxation data. We have been guided by the principle of Occam's razor, namely that the simplest model that matches the data is probably the best. The well known tetrahedral jumps of the O–H bonds on the ice I_h lattice and C_2 symmetry jumps of the O–H bonds observed for crystalline hydrates provide a logical basis for the C2TET model.

The comparison of theoretical and experimental deuterium T_1 data for $^2\text{H}_2\text{O}$ -synthesized kanemite and $^2\text{H}_2\text{O}$ -hydrated Zeolite A shows that the C2TET model works well, and is the only one that successfully accounts for the magnetic field dependence of T_1 values observed experimentally at ambient and higher temperatures. FTIR and variable temperature deuterium lineshape analyses of both materials are also consistent with the C2TET model. The experimental deuterium T_2 data are imprecise due to exchange effects. Based on the T_1 relaxation and lineshape analysis, the kinetic activation parameters for the $^2\text{H}_2\text{O}$ -hydrated Zeolite A are $\Delta H_{\text{tet}}^\ddagger = +17$ kJ/mol, $\Delta S_{\text{tet}}^\ddagger = -109$ J/(mol K), $\Delta H_{\text{C}_2}^\ddagger = +19$ kJ/mol, and $\Delta S_{\text{C}_2}^\ddagger = -20$ J/(mol K). For the $^2\text{H}_2\text{O}$ -

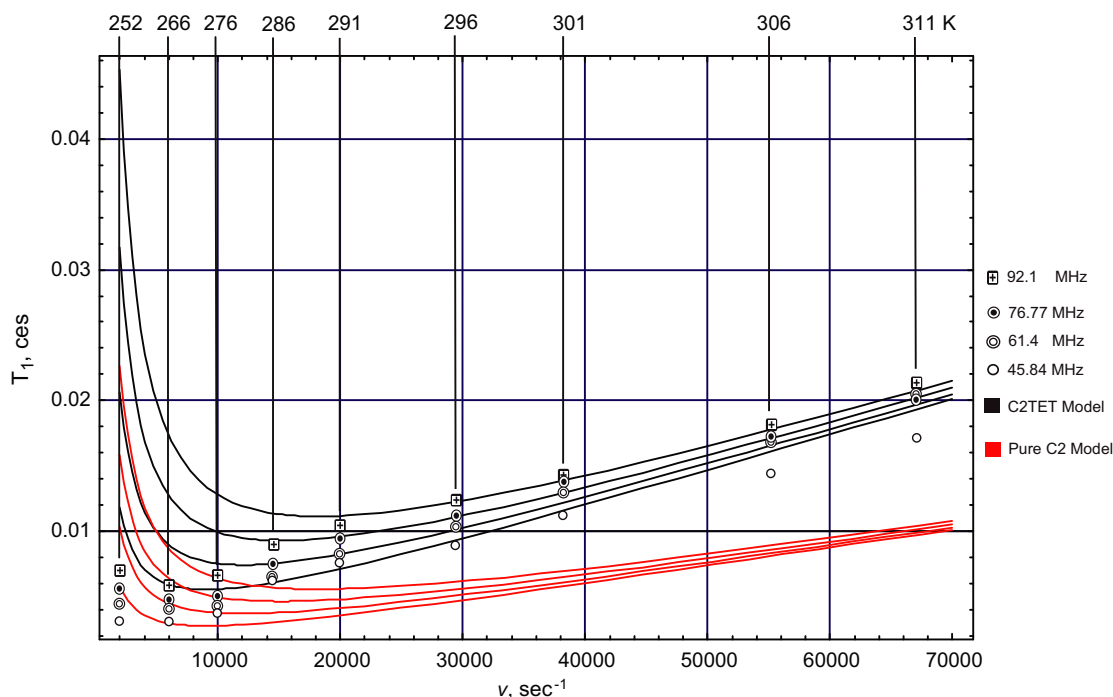


Fig. 18. The low temperature experimental T_1 data for the sharp central resonance of $^2\text{H}_2\text{O}$ -hydrated Zeolite A are plotted on the background of the best fit theoretical T_1 values for the C2TET model (black theoretical curves, $\chi_{\text{tet}} = \chi_{\text{C}_2} = 0.5$, $\nu = k_{\text{tet}}$, $k_{\text{C}_2}/k_{\text{tet}} = 25,833$) and the pure C_2 jump model (red theoretical curves, where we have used $k_{\text{C}_2} = 25,833 \nu$ so direct comparison is possible with the C2TET model) for deuterium frequencies of 46.03, 61.42, 76.77, and 92.13 MHz. For the C2TET model, the ratio of $k_{\text{C}_2}/k_{\text{tet}}$ was assumed to be constant throughout the temperature range, and was chosen to yield the best possible fit of the resulting theoretical curves to the experimental data. Curves for pure tetrahedral jumps and pure isotropic rotational diffusion are off the scale of this figure. There was no way to fit the experimental data with the isotropic rotational diffusion model or the perfect tetrahedral jump model. The best fit was obtained with $q_{\text{cc}} = 200$ kHz and $\eta = 0$.

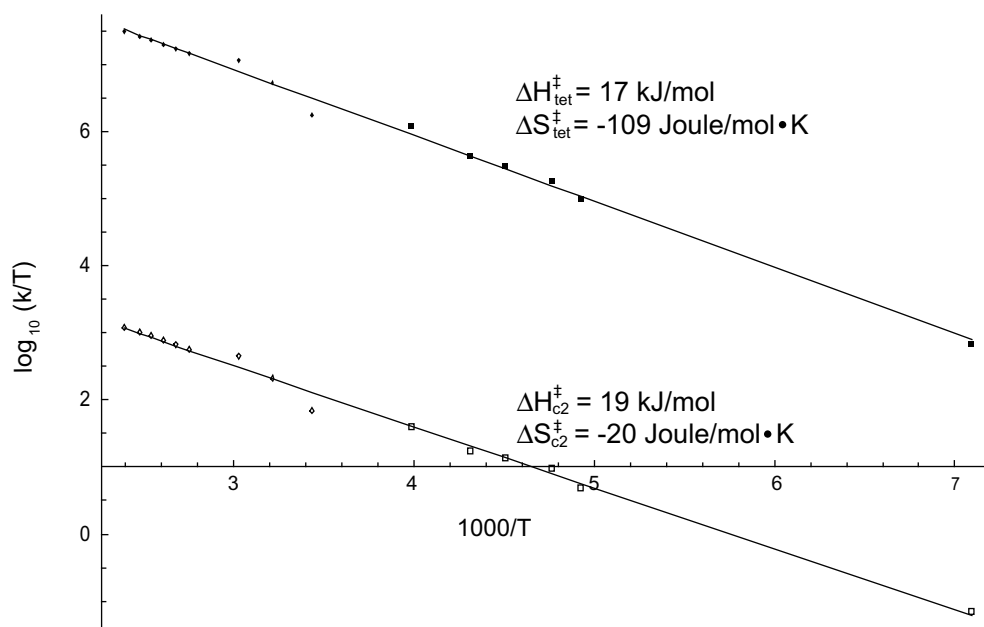


Fig. 19. Eyring plots [33] of the k_{C_2} and k_{tet} values in $^2\text{H}_2\text{O}$ -hydrated Zeolite A obtained from the simulations in Fig. 12 (low temperature data) and from the T_1 data from Fig. 17 (high temperature data). $\Delta H_{\text{tet}}^{\ddagger} = +17$ kJ/mol, $\Delta S_{\text{tet}}^{\ddagger} = -109$ J/(mol K), $\Delta H_{\text{C}_2}^{\ddagger} = +19$ kJ/mol, and $\Delta S_{\text{C}_2}^{\ddagger} = -20$ J/(mol K).

synthesized kanemite, the kinetic activation parameters are $\Delta H_{\text{tet}}^{\ddagger} = +23$ kJ/mol, $\Delta S_{\text{tet}}^{\ddagger} = -69$ J/(mol K), $\Delta H_{\text{C}_2}^{\ddagger} = +23$ kJ/mol, and $\Delta S_{\text{C}_2}^{\ddagger} = -11$ J/(mol K). For both samples the C_2 jumps of the $\text{O}-^2\text{H}$ bonds are much faster than the tetrahedral jumps at all temperatures.

Our goal in future work is to uncover more details of the dynamics in these and other systems, in particular the details of the exchange between the water populations experiencing C_2 and tetrahedral jumps of their $\text{O}-\text{H}$ bonds. Other questions include the role of the cation in such systems and whether the C2TET mod-

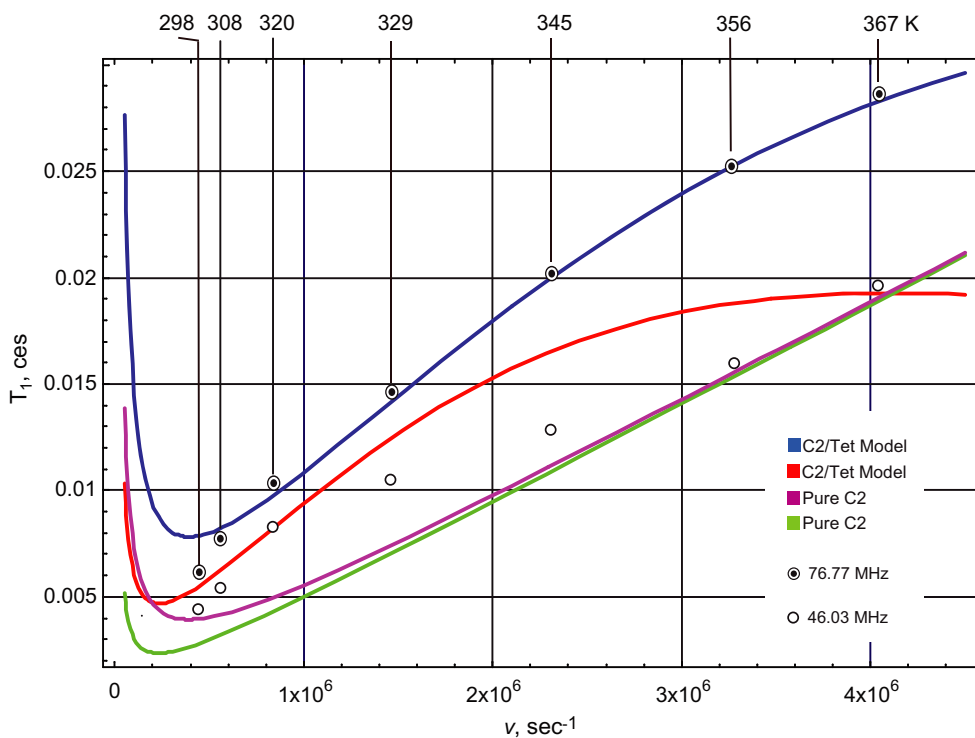


Fig. 20. The high temperature experimental T_1 data for the sharp central resonance of $^2\text{H}_2\text{O}$ -synthesized kanemite at 46.03 (red curve) and 76.77 MHz (blue curve) plotted on the background of the theoretical T_1 values the C2TET model ($\chi_{\text{tet}} = \chi_{\text{C}_2} = 0.5$, $\nu = k_{\text{tet}}$, $k_{\text{C}_2}/k_{\text{tet}} = 1000$). The ratio of $k_{\text{C}_2}/k_{\text{tet}}$ (assumed to be constant throughout the temperature range) was chosen to yield the best possible fit of the resulting theoretical curves to the experimental data. Plots of the pure C_2 model, calculated for $k_{\text{C}_2} = 1000 \nu$ so that the T_1 values can be expressed in terms of k_{tet} at 46.03 (green) and 76.77 MHz (purple) are shown for comparison. Curves for pure tetrahedral jumps and pure isotropic rotational diffusion are off the scale of this figure. There was no way to fit the experimental data with the isotropic rotational diffusion model or the pure tetrahedral jump model. The best fit for the C2TET model was obtained with $q_{\text{cc}} = 210$ kHz and $\eta = 0.1$. (For interpretation of the references to color in this figure legend, the reader is referred to the web version of this paper.)

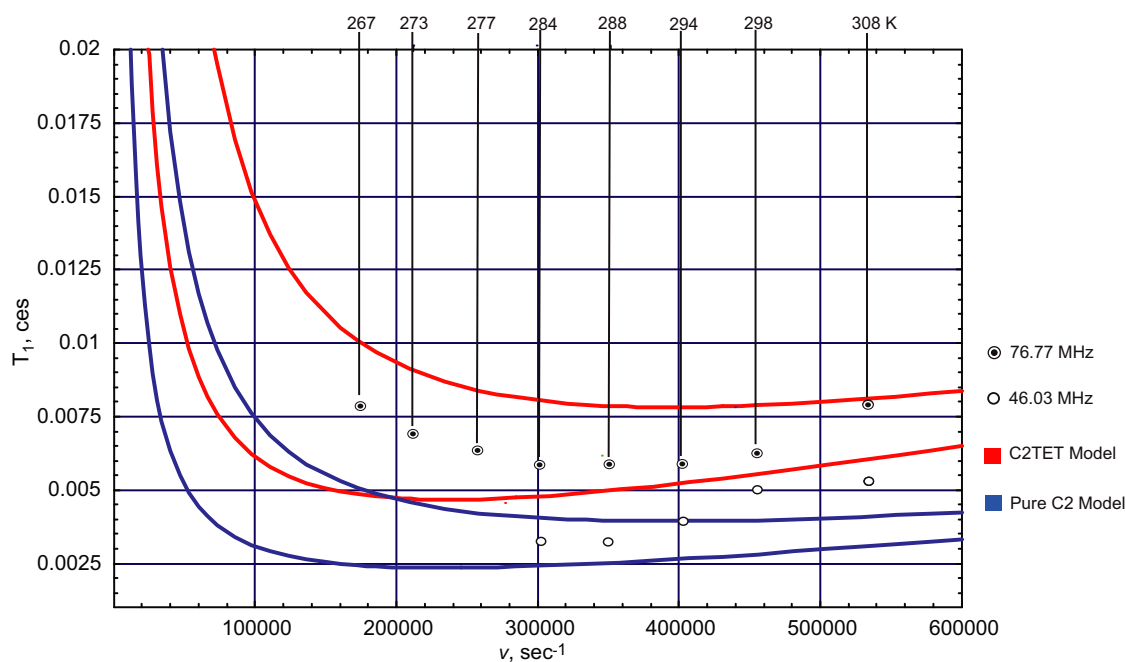


Fig. 21. Lower temperature experimental T_1 data for the sharp central resonance of $^2\text{H}_2\text{O}$ -synthesized kanemite at 46.03 and 76.77 MHz (red curves) plotted on the background of the theoretical C2TET T_1 values ($\chi_{\text{tet}} = \chi_{\text{C}_2} = 0.5$, $\nu = k_{\text{tet}}$, $k_{\text{C}_2}/k_{\text{tet}} = 1000$). The ratio of $k_{\text{C}_2}/k_{\text{tet}}$ (assumed to be constant throughout the temperature range) was chosen to yield the best possible fit of the resulting theoretical curves to the experimental data obtained at higher temperatures, Fig. 20. Plots of the pure C_2 model (blue curves), calculated for $k_{\text{C}_2} = 1000 \nu$ at 46.03 (lower) and 76.77 MHz (upper) are shown for comparison. Curves for pure tetrahedral jumps and pure isotropic rotational diffusion are off the scale of this figure. There was no way to fit the experimental data with the isotropic rotational diffusion model or the perfect tetrahedral jump model. The best fit was obtained with $q_{\text{cc}} = 210$ kHz and $\eta = 0.1$. (For interpretation of the references to color in this figure legend, the reader is referred to the web version of this paper.)

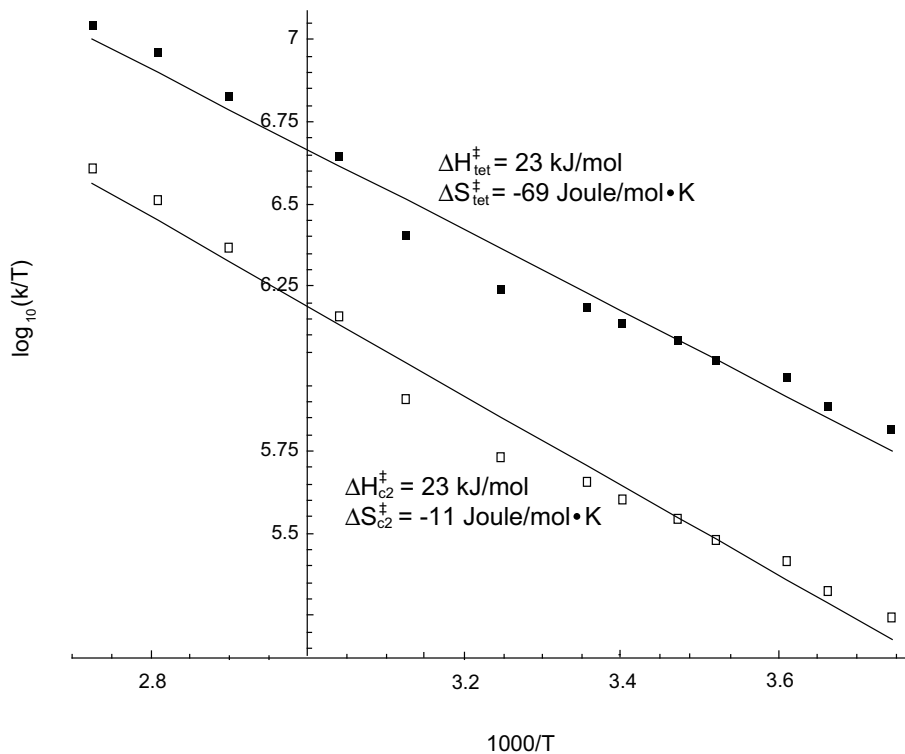


Fig. 22. Eyring plots [33] of the tetrahedral jump rate k values for $^2\text{H}_2\text{O}$ -synthesized kanemite obtained from Figs. 20 and 21. The activation parameters are $\Delta H_{\text{tet}}^\ddagger = +23$ kJ/mol, $\Delta S_{\text{tet}}^\ddagger = -69$ J/(mol K), $\Delta H_{\text{C}_2}^\ddagger = +23$ kJ/mol, and $\Delta S_{\text{C}_2}^\ddagger = -11$ J/(mol K). The ΔH^\ddagger values are the same because it was assumed that $k_{\text{C}_2}/k_{\text{tet}}$ is constant and equal to 1000 in Figs. 20 and 21.

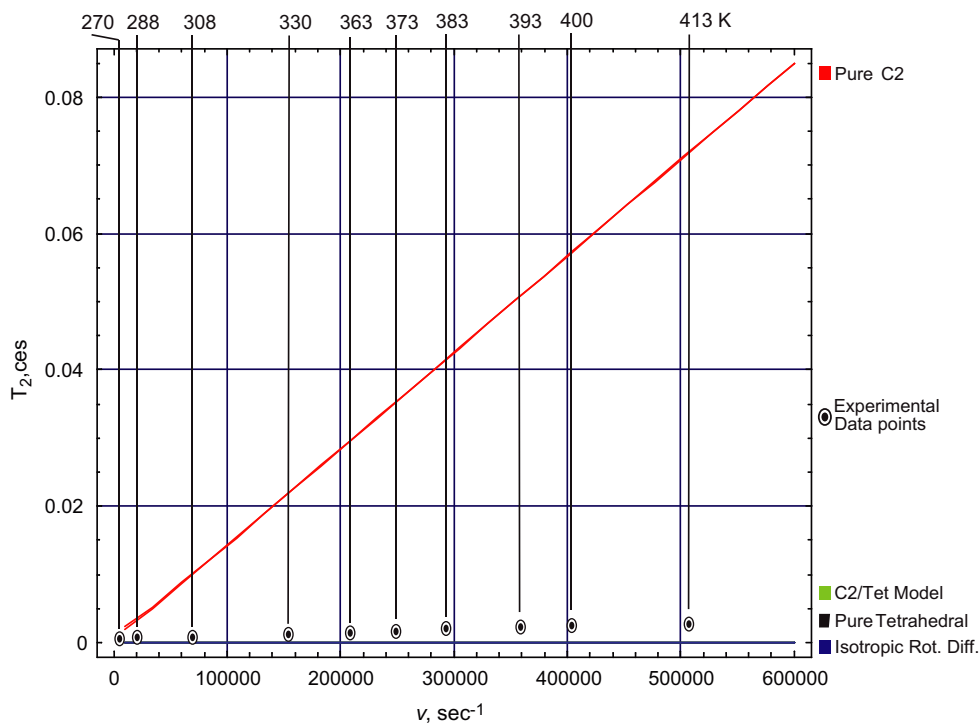


Fig. 23. The experimental T_2 data (CPMG 2 π pulses, double echo) for the sharp central resonance of $^2\text{H}_2\text{O}$ -hydrated Zeolite A at 76.77 MHz plotted on the background of the theoretical T_2 values calculated for isotropic rotational diffusion ($\nu = 6 D_{\text{rot}}$, blue curves), ideal tetrahedral jumps ($\nu = k$, black curves), and C2TET model ($\nu = k_{\text{tet}}$, $k_{\text{C}_2}/k_{\text{tet}} = 25,833$, green curves). The ratio of $k_{\text{C}_2}/k_{\text{tet}}$ was the same as used in Figs. 17 and 18. It is also used in the plot of the “pure” C_2 curve (red curve), which is expressed in terms of $\nu = k_{\text{tet}}$ (for example, if $\nu = 1 \times 10^5 \text{ s}^{-1}$, $k_{\text{C}_2} = 2.5833 \times 10^9 \text{ s}^{-1}$). The temperatures shown in the figure are placed at the same $\nu = k$ values as used in the plots of the T_1 data made to fit the C2TET model in Figs. 17 and 18. The T_2 values for isotropic rotational diffusion of bulk liquid water are off the scale of this plot, over two orders of magnitude longer than the experimental values. The isotropic rotational diffusion coefficient range shown in the plot corresponds to supercooled liquid water at 200 K and extremely high pressure [8]. (For interpretation of the references to color in this figure legend, the reader is referred to the web version of this paper.)

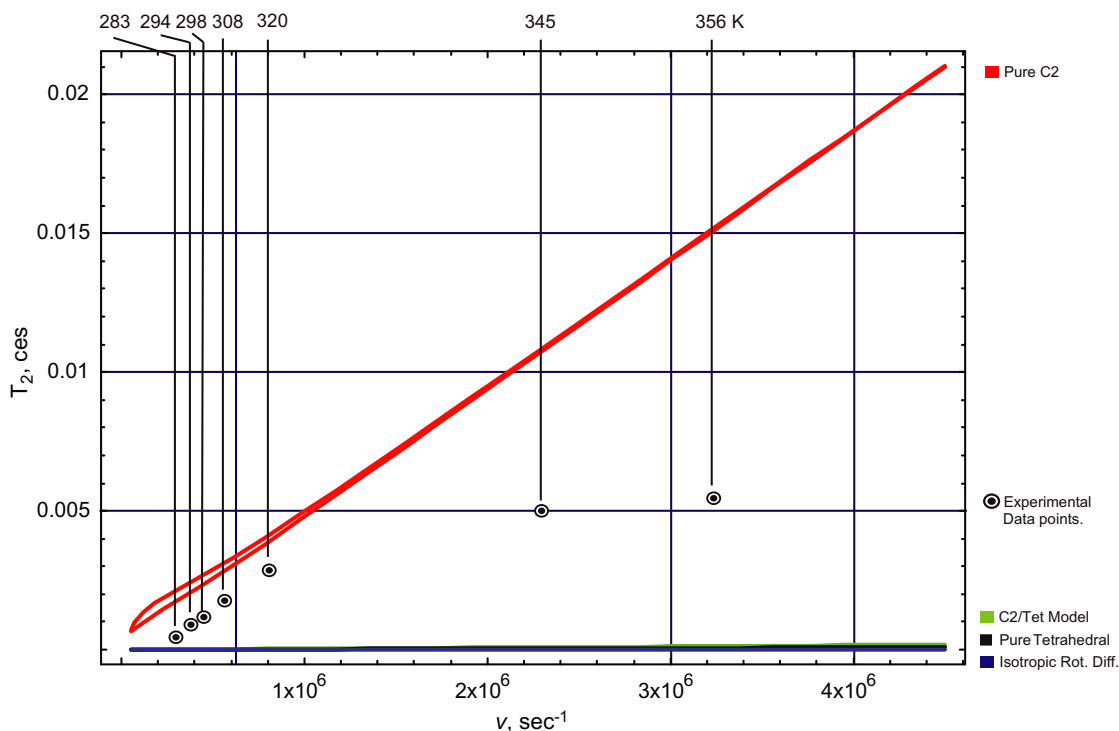


Fig. 24. The experimental T_2 data (CPMG 2 π pulses, double echo) for the sharp central resonance of $^2\text{H}_2\text{O}$ -synthesized kanemite at 76.77 MHz plotted on the background of the theoretical T_2 values calculated for isotropic rotational diffusion ($\nu = 6 D_{\text{rot}}$, blue curves), ideal tetrahedral jumps ($\nu = k$, black curves), and C2TET model ($\nu = k_{\text{tet}}$, $k_{\text{C}_2}/k_{\text{tet}} = 1000$, green curves) at both frequencies. The ratio of $k_{\text{C}_2}/k_{\text{tet}} = 1000$ (assumed to be constant throughout the temperature range) was the same as used in Figs. 20 and 21, and is also used in the plot of the “pure” C_2 curve (red curve), which is expressed in terms of $\nu = k_{\text{tet}}$ (for example, at $\nu = 1 \times 10^6 \text{ s}^{-1}$, $k_{\text{C}_2} = 1 \times 10^9 \text{ s}^{-1}$). The temperatures shown in the figure are placed at the same ν values as used in the plots of the T_1 data constructed to the C2TET model in Figs. 20 and 21. The T_2 values for isotropic rotational diffusion of bulk liquid water are off the scale of this plot, over two orders of magnitude longer than the experimental values. The isotropic rotational diffusion coefficient range shown in the plot corresponds to supercooled liquid water at 200 K and extremely high pressure [8]. (For interpretation of the references to color in this figure legend, the reader is referred to the web version of this paper.)

el can successfully describe deuterium T_1 relaxation in other hydrated materials.

Acknowledgments

We thank Burkhard Geil for his generous help, including detailed and illuminating discussions as well as experimental determination of T_1 data for kanemite at low temperatures. We thank Attila Szabo and Matthew Augustine for clarifying discussions. We also thank the Pennsylvania State University and the Department of Chemistry for their support.

References

- [1] A.J. Benesi, M.W. Grutzeck, B. O'Hare, J.W. Phair, Room temperature solid surface water with tetrahedral jumps of ^2H nuclei detected in $^2\text{H}_2\text{O}$ -hydrated porous silicates, *J. Phys. Chem. B* 108 (2004) 17783–17790.
- [2] A.J. Benesi, M.W. Grutzeck, B. O'Hare, J.W. Phair, Room-temperature ice-like water in kanemite detected by ^2H NMR T_1 relaxation, *Langmuir* 21 (2005) 527–529.
- [3] Asay DB, Kim SH, Evolution of the adsorbed water layer structure on silicon oxide at room temperature, *J. Phys. Chem. B* 109 (2005) 16760–16763.
- [4] We assume the sample is diamagnetic.
- [5] M. Mehring, Internal spin interactions & rotations in solids, in: D.M. Grant, R.K. Harris (Eds.), *Encyclopedia of NMR*, Wiley, Chichester, 1996, pp. 2585–2603.
- [6] B. Geil, T.M. Kirschgen, F. Fujara, Mechanism of proton transport in hexagonal ice, *Phys. Rev. B* 72 (2005). 014304/1–014304/10.
- [7] H.W. Spiess, Deuteron spin alignment: a probe for studying ultraslow motions in solids and solid polymers, *Chem. Phys. Lett.* 72 (1980) 6755–6762.
- [8] E.W. Lang, H.-D. Ludemann, L. Piculell, Nuclear magnetic relaxation rate dispersion in supercooled heavy water under high pressure, *J. Chem. Phys.* 81 (1984) 3820–3827.
- [9] B. Geil, F. Fujara, H. Sillecu, ^2H NMR time domain analysis of ultraslow reorientations in supercooled liquids, *J. Magn. Res.* 130 (1998) 18–26.
- [10] X. Tang, A. Benesi, A ^{13}C spin–lattice relaxation study of the effect of substituents on rigid-body rotational diffusion in methylene chloride solution and in the solid state, *J. Phys. Chem.* 98 (1994) 2844–2847.
- [11] R.J. Wittebort, M.G. Usha, D.J. Ruben, D.E. Wemmer, A. Pines, *J. Am. Chem. Soc.* 110 (1988) 5668–5671.
- [12] A. Weiss, N. Weiden, Deuteron Magnetic Resonance in Crystal Hydrates, in: J.A.S. Smith (Ed.), *Advances in Nuclear Quadrupole Resonance*, vol. 4, Heyden, London, 1980, pp. 149–248.
- [13] L.W. Reeves, The Study of Water in Hydrate Crystals by Nuclear Magnetic Resonance, in: W. Emsley, J. Feeney, L.H. Sutcliffe (Eds.), *Progress in NMR Spectroscopy*, vol. 4, Pergamon, Oxford, 1969, pp. 193–234.
- [14] T.M. Kirschgen, M.D. Zeidler, B. Geil, F. Fujara, A deuteron NMR study of the tetrahydrofuran clathrate hydrate parts I & II, *Phys. Chem. Chem. Phys.* 5 (2003) 5243–5252.
- [15] D.A. Torchia, A. Szabo, Spin–lattice relaxation in solids, *J. Magn. Res.* 49 (1982) 107–121.
- [16] H.W. Spiess, Rotation of molecules and nuclear spin relaxation, in: P. Diehl, E. Fluck, R. Kosfeld (Eds.), *NMR, Basic Principles and Progress*, vol. 15, Springer-Verlag, New York, 1978, pp. 59–214.
- [17] G. Lipari, A. Szabo, Model-free approach to the interpretation of nuclear magnetic resonance relaxation in macromolecules. 1. Theory and range of validity, *J. Am. Chem. Soc.* 104 (1982) 4546–4559.
- [18] In our earlier work, we omitted the factor of 2 so the spectral densities and T_1 values were also off by a factor of two.
- [19] D.E. Woessner, Brownian motion and correlation times, in: D.M. Grant, R.K. Harris (Eds.), *Encyclopedia of Nuclear Magnetic Resonance*, Wiley, Chichester, 1996, pp. 1068–1084.
- [20] J. Sudmeier, S. Anderson, J. Frye, Calculation of nuclear spin relaxation times, *Concepts in Magnetic Resonance* 2 (1990) 197–212.
- [21] The spectral densities provided as supplemental information in our previous publications, 1 and 2 above, are half of the correct value shown in Eqs. (3a)–(3c).
- [22] L.A.J. Garvie, B. Devouard, T.L. Groy, F. Camara, P.R. Buseck, Crystal structure of kanemite, $\text{NaHSi}_2\text{O}_5 \cdot 3\text{H}_2\text{O}$, from the Aris phonolite, Namibia, *Am. Mineral.* 84 (1999) 1170–1175.
- [23] V. Gramlich, W.M. Meier, The crystal structure of hydrated NaA: a detailed refinement of a pseudosymmetric Zeolite structure, *Z. Kristallographie* 133 (1971) 134–149.

- [24] No liquid state water was detected in the experiments, but it is possible that small mole fractions of liquid water in fast exchange with the solid water may have been masked by the much slower relaxation rate. For example, at room temperature $T_{1\text{liq}} \approx 0.40 \text{ s}^{-1}$, so $(1/T_1)_{\text{obsd}} = \chi_{\text{liq}} (2.5 \text{ s}^{-1}) + \chi_{\text{sol}} (1/T_1)_{\text{sol}}$ with $(1/T_1)_{\text{sol}} > 100 \text{ s}^{-1}$.
- [25] This assumption anticipates the results obtained from experiment that show $k_{C_2} \gg k_{\text{tet}}$. It also allows us to avoid assumptions about the activation energies for k_{C_2} and k_{tet} at this point in the discussion.
- [26] T.L. Brown, H.E. LeMay, B.E. Bursten, Chemistry, tenth ed., The Central Science, Pearson, Upper Saddle River, NJ, 2006. pp. 269.
- [27] S. Hayashi, Solid-state NMR study of the locations and dynamics of interlayer cations and water in kanemite, *J. Mater. Chem.* 7 (1997) 1043–1048.
- [28] J.E. Readman, N. Kim, M. Ziliox, C.P. Grey, ^{17}O MQMAS studies of Na-A and Ca-A, *Chem. Commun.* (2002) 2808–2809.
- [29] We thank Burkhard Geil for the low temperature T_1 data.
- [30] Y. Huang, Z. Jiang, W. Schwieger, A vibrational spectroscopic study of kanemite, *Microporous Mesoporous Mater.* 26 (1998) 215–219.
- [31] Z.-F. Wei, Y.-H. Zhang, L.-J. Zhao, J.-H. Liu, X.-H. Li, Observation of the first hydration layer of isolated cations and anions through the FTIR-ATR difference spectra, *J. Phys. Chem. A* 109 (2005) 1337–1342.
- [32] A.J. Vega, Z. Luz, Quadrupole echo distortion as a tool for dynamic NMR: application to molecular reorientation in solid trimethylamine, *J. Chem. Phys.* 86 (1987) 1802–1813.
- [33] H. Eyring, The activated complex in chemical reactions, *J. Chem. Phys.* 3 (1935) 107–115.
- [34] C.P. Lindsey, G.D. Patterson, Detailed comparison of the Williams–Watts and Cole–Davidson functions, *J. Chem. Phys.* 73 (1980) 3348–3357.
- [35] J.C. Hindman, A.J. Zielen, A. Svirmickas, M. Wood, Relaxation processes in water. Spin–lattice relaxation of the deuteron in D_2O and oxygen-17 in $H_2^{17}O$, *J. Chem. Phys.* 54 (1971) 621–634.
- [36] D.E. Woessner, Relaxation effects of chemical exchange, in: D.M. Grant, R.K. Harris (Eds.), *Encyclopedia of Nuclear Magnetic Resonance*, Wiley, Chichester, 1996, pp. 4018–4028.
- [37] We also obtained a few T_2 data values at 46.03 MHz to check for magnetic field dependence. None was found within the experimental error.